UNIVERSITY OF NAIROBI
College of Architecture and Engineering
Institute of Nuclear Science and Technology

Design and Characterisation of an Electrohydrodynamic Multinozzle Atomizer for Thermal Desalination Processes

By
Mwaura Anselim Mwangi
S56/61782/2013
BSc. Mechatronic Engineering, JKUAT

A thesis submitted in partial fulfilment for the degree of Master of Science in Nuclear Science in the Institute of Nuclear Science and Technology in the University of Nairobi, Kenya.

Declaration

This thesis is my original work and has not been presented for a degree in any other university.

Signature ……. Date…….
Mwaura, Anselim Mwangi

Supervisors' Approval

This thesis has been submitted for examination with our knowledge as university supervisors

Prof. Michael J. Gatari Signature ……
Institute of Nuclear Science and Technology Date…….
University of Nairobi, Kenya.

Prof. Jan C. M. Marijnissen Signature ……
University of Nairobi and Florida Date…….
Kenya and United States of America.

Dr. Luewton L. F. Agostinho Signature ……
NHL, University of Applied Sciences Date…….
Leeuwarden, Netherlands.

Dedication

I dedicate this research work to my parents, Erastus and Anne Mwaura as well as my brothers; Muiruri and Kibe. Neither can I forget Prof. Michael Gatari, Prof. Jan Marijnissen and Dr. Luewton Agostinho and their families. May the Almighty God bless you abundantly.

Acknowledgements

A significant number of people have contributed to the work presented in this thesis and for this it is now my pleasure to thank them.

First of all, I wish to take this opportunity to offer my tokens of appreciation to the God Almighty, to whom I owe my life, health and wisdom to undertake this research.

I am grateful to Centre of Expertise Water Technology (CEW), Water Application Centre (WAC) and High Voltage Water (HV Water) fraternities in The Netherlands, for giving me a fellowship to carry out this research. It was my pleasure working with you.

I am indebted to the University of Nairobi through Institute of Nuclear Science and Technology (INST) for awarding me with the scholarship as well as supporting the fellowship.

I also acknowledge the support by International Science Programme (ISP), Uppsala, Sweden, for logistics funding and providing the necessary support throughout the research period. Also for facilitating various conferences, workshops and trainings throughout my research, I am really grateful.

I am greatly indebted to the Kenya Nuclear Electricity Board (KNEB) who paid for my tuition fee and stipend.

I must also extend my sincere gratitude to Prof. Michael J. Gatari, Prof. Jan C. M. Marijnissen and Dr. Luewton L. F. Agostinho whose mentoring, invaluable advice, show of confidence and keen insights were integral to the success of this research. They have also successfully stimulated my interest in the area of electrospray desalination process through their own enthusiasm for this subject.

My heart felt gratitude goes to my fiancée, Lilian Gathoni, for all the encouragements, support and ideas throughout the research period.

Special thanks must go to my family, friends, fellow classmates and INST staff who have provided me with invaluable support continuously throughout the research period and motivation that has seen me achieve my intellectual abilities to take on the challenges facing our world and offer a solution to the water scarcity the world experiences.

Table of Contents

List of Tables

List of Figures

Acronyms and Abbreviations

DC	Direct Current
EHDA	Electrohydrodynamic Atomization
GOK	Government of Kenya
IAEA	International Atomic Energy Agency
ICP-MS	Inductively Coupled Plasma Mass Spectrometry
JMP	Joint Monitoring Programme for Water Supply and Sanitation
KIHBS	Kenya Integrated Household Budget Survey
MDG	Millennium Development Goal
MED	Multi-Effect Distillation
MSF	Multi-Stage Flash Distillation
PE	Polyethylene
POM	Polyoxymethylene
SDG	Sustainable Development Goal
TDM	Total Dissolved Minerals
TXRF	Total Reflection X-ray Fluorescence
PS	Power Supply
RO	Reverse Osmosis
RSD	Relative Standard Deviation
UN	United Nations

Abstract

Water is one of the three basic necessities (Air, water and food) of life on earth. Access to adequate quantities of safe and fresh water for drinking, domestic, commercial, agricultural and industrial application is vital to human, health and ecosystem well-being as well as to achieving sustainable economic development.

Worldwide water scarcity, climate change, bad management of available water sources, population and industrial growth are pressing the world to come up with innovative ways of sourcing for clean drinking water. Seawater desalination is a promising technology since the abundance of seawater makes it one of the favourable sources for desalination. Among many other desalination processes, multi effect distillation is known for its robustness and high production; however it still delivers a recovery ratio (total fresh water volume per total inlet volume) of only 10%. There is therefore need to increase its efficiency. The objective of this research work was to design and characterise a multinozzle atomizer which uses electrohydrodynamic atomization, also known as electrospray, to create small sized electrically charged droplets to improve the efficiency of thermal desalination processes.

This research work involved the study of the attraction of droplets to the tube, designing of the multinozzle atomizer prototype, computational modelling to check the process parameters, simulating the complete design and characterising the working conditions of the device. Bench scale experiments were carried out to investigate the behaviour of the electrohydrodynamic multinozzle atomizer and the properties of the droplets. Additionally, a second prototype was designed and studied to eliminate the limitations experienced by the first one.

The design and characterisation of the electrohydrodynamic multinozzle atomizer was done. It was observed that there was reduction in droplet diameter and the droplets of the outermost nozzles had a wider dispersion compared to the inner nozzles with increase in voltage. The results of the bench scale experiments matched with both the particle trajectories and electric field modelling. The elemental concentration of the seawater did not change significantly with the application of high voltage during the electrospray process.

1. INTRODUCTION

1.1 Background

Water is the most important natural resource and the backbone of growth and prosperity for mankind. According to El-Dessouky and Ettouney (2002) and Micale et al. (2009), the area on earth covered by water is approximately 70% of the planet surface area which is about 1.4 x 10^9 km^2. The percentage of salt water of all the water on earth is 97.5%. The remaining 2.5% is fresh water of which 80% of it, is soil moisture or frozen in the icecaps. Both forms are not easily accessible for use by humans. The remaining quantity which is about 0.5% of all the water on earth is believed to be sufficient to support life that depends on fresh water. Unfortunately, this water is not evenly distributed throughout the planet (El-Dessouky and Ettouney, 2002). Consequently, much of the world is now facing or will soon face chronic shortage of potable water without which, life will not be possible. With the ever growing world population, the availability of fresh water will decrease even further.

The world through the United Nations organization came up with initiatives to improve on the water scarcity situation. These initiatives were known as Millennium Development Goals (MDGs). The Seventh MDG aimed at ensuring environmental sustainability. The target in sub-article C was to reduce by half the world population without sustainable access to basic sanitation and safe drinking water by the year 2015 (MDGs, 2014). The Joint Monitoring Programme for Water Supply and Sanitation (JMP) published that the MDGs target for drinking water was obtained in 2010; the world population without access to potable drinking water sources was more than halved (from 24% to 11%) since 1990 (WHO, 2012). In 2015, United Nations organization reviewed the MDGs and adopted a set of global goals known as Sustainable Development Goals (SDGs). The Sixth SDG aims at ensuring access to water and sanitation for all of the world population. It targets to achieve worldwide and equitable access to potable and safe drinking water for all by the year 2030 (SDGs, 2015). In spite of the increase from 76 per cent to 91 per cent between 1990 and 2015 of the world population using an improved and safe drinking water source (SDGs, 2015); there is still need to reduce the population without sustainable access to basic sanitation and safe drinking water.

Kenya, in particular, is a water scarce country (GOK, 2007). The Water Services Strategy in Kenya indicates that the situation is poor with approximately 57% of all Kenyan households are using water from sources that are considered safe. Access to sustainable safe water is estimated at 60% in the urban setting. Additionally, the percentage of those who have access

to safe water sources in the urban poor settlements drops to low levels of 20% yet half of the urban population lives there. Access to sustainable safe water in the rural setting is estimated at 40% (KIHBS, 2005 and 2006). In some areas, people are forced to walk long distances just to obtain adequate water to sustain life. Consequently, they endure health consequences and thus they do not have the opportunity to develop their resources and capabilities to achieve economic independence (WHO, 2012). This challenge has created opportunities for investigation and improvement of non-traditional ways of obtaining fresh water such as desalination.

Desalination is seen as an important solution to the water scarcity problem by producing safe water and if used efficiently, it may be used to provide water to satisfy the needs of ever demanding and growing world population (WHO, 2011; WWF, 2007). The process entails the separation of salt and fresh water from sea or brackish water. However, desalination of seawater is an energy intensive process according to Ettouney and Wilf (2009) and WHO (2011). It is only used after careful consideration of cheaper alternatives and where there is a pressing water scarcity situation. Therefore, there is a need to come up with desalination technologies with high energy efficiency.

Desalination processes can be classified based on thermal processes such as multi stage flash distillation (MSF), multi effect distillation (MED) and thermo vapour compression distillation (TVC) or membrane separation methods including electrodialysis (ED) and reverse osmosis (RO) (El-Dessouky and Ettouney, 2002). Jingwei et al. (2010) proved that a careful selection of the atomization method in thermal desalination can produce recovery rates as high as 95%. Amongst the thermal desalination processes which have a lower energy requirement when compared to membrane separation, multi effect distillation has the least (Ettouney and Wilf, 2009). Nevertheless, multi effect distillation still has a low recovery ratio of about 10%. Recovery ratio is defined as the ratio of the amount of total fresh water volume per total inlet volume. It has been investigated that when multi effect distillation is coupled with electrohydrodynamic atomization, there is an increase in energy efficiency and spray evaporation of about 40% (Agostinho, 2013). Agostinho (2013) performed experiments with a 5-nozzle electrohydrodynamic atomizer coupled with a single effect distillation chamber. This being a very promising hybrid technology, it needs to be out-scaled to increase the output.

1.2 Problem Statement

A major problem in the society is the provision of sufficient quantities of safe water. Currently, the world's population is suffering from serious fresh water shortage with about 40% experiencing the shortage (SDGs, 2015) and this percentage is expected to increase by the year 2025 to more than 60% (El-Dessouky and Ettouney, 2002). By the year 2040, it is projected that the demand in the world for fresh water will surpass it availability at that time (Micale et al., 2009). This is as a result of the increased economic activities, rapid increase of population, pollution of the available fresh water resources, changes in the lifestyle and global climatic changes among other reasons.

In Kenya, at present, 43% of the total population is suffering from fresh water scarcity (KIHBS, 2005 and 2006). The situation is further worsened by drying up of fresh water sources, increased human activities, deforestation, pollution of the remaining water sources and climate change.

There is therefore need to develop means of providing safe and fresh water using an energy efficient technique. Single effect distillation being the least energy intensive process of thermal desalination technologies can be used to solve the water scarcity problem. Therefore, there is need to improve its efficiency by improving and out scaling the development work initiated by Agostinho (2013) and Brouwer (2011).

1.3 Justification of the Research

The possibility to provide an energy efficient method of sourcing for large quantities of fresh water and a higher recovery ratio motivated outscaling of Agostinho's (2013) and Brouwer's (2011) desalination prototype system. The system had 5 nozzles but since in electrospray, the desired droplet size is a function of the nozzle inner diameter, increasing the number of nozzles will increase the liquid output at a constant flow rate per nozzle in simple jet mode. Additionally, electrospray will minimise the energy for atomization and thus increase the energy efficiency of the system. However, simulation of the envisioned model and a laboratory prototype were required where proofing tests of the expected benefits was carried out. This required minimal investment while the benefits from the experimental success were much more.

1.4 Scope of the Research

The research focused on the bench scale study of the characteristics of the electrohydrodynamic multinozzle atomizer for a single effect chamber. This involved getting acquainted with the electrospray technology by performing experiments with a 10 nozzle atomizer coupled with an evaporator.

It also sought to determine the suitable model to balance the process parameters and to simulate the particle trajectories, which gave insights in the behaviour of the droplets. This helped in predicting adjustments leading to better target deposition of the actual complete design and for the best multinozzle atomizer.

The electrosprayed seawater was analysed to assess whether there was trace element contamination in the system.

It sought to investigate the required potential and the appropriate distance needed to attract the charged electrosprayed droplets to a tube.

It sought to determine the most suitable design of the optimal multinozzle atomizer configuration and used the computational models for optimization of the optimal multinozzle system.

1.5 Objectives

1.5.1 Main Objective

The main objective was to design, develop and study the characteristics of an electrohydrodynamic multinozzle atomizer for thermal desalination processes.

1.5.2 Specific Objectives

1) To develop computational models to check the process parameters.
2) To assemble and test the electrohydrodynamic multinozzle atomizer.
3) To study and characterise the electrohydrodynamic multinozzle atomizer.
4) To design the optimal multinozzle atomizer configuration and use the computational models for optimization of the optimal multinozzle system.
5) To investigate any changes in concentrations of selected trace elements after process through the electrospray system using Inductively Coupled Plasma Mass Spectrometry (ICP-MS) and Total Reflection X-ray Fluorescence (TXRF) methods.

2. LITERATURE REVIEW

2.1 Water

The water cycle on earth makes the total amount of water constant over time. Water evaporates from the vegetation on the earth surface, seas and surface waters among other sources to the atmosphere. Water vapour cools and condenses to form water droplets which accumulate to form clouds. When enough water condenses, the water droplets become heavy which in turn falls as rainfall. Rain water feeds into underground waters, surface waters and seas (Micale et al., 2009; El-Dessouky and Ettouney, 2002). Water can be classified according to total dissolved solids (Table 2.1).

Table 2.1: Water classification based on Total Dissolved Minerals

Type	Total Dissolved Minerals (TDM) (in parts per million, ppm)
Fresh water	Up to 1,500
Brackish water	1,500 – 10,000
Salt water	> 10,000
Seawater	10,000 – 45,000
Standard seawater	35,000

Adopted from Micale et al., (2009).

Fresh water differs from brackish or seawater by the extent of the minerals that they contain. The main ions found in seawater include K^+, Na^+, Mg^{2+}, Ca^{2+}, Cl^- and $(S0_4)^{2-}$ (Figure 2.1). All other ions are present but in smaller concentrations.

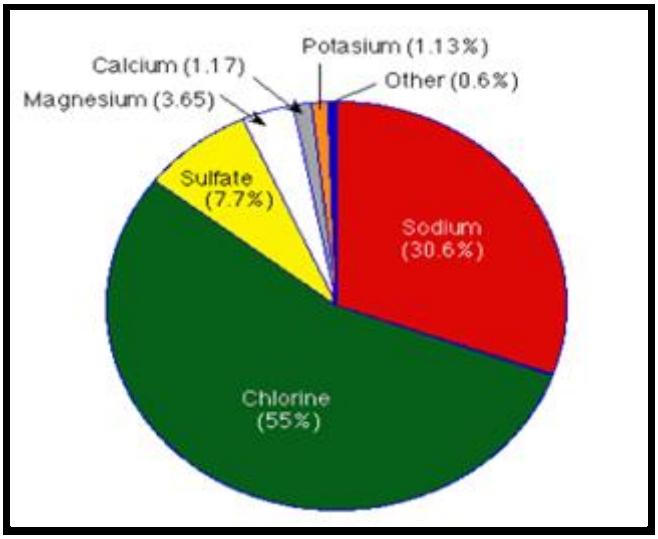

Adapted from (El-Dessouky and Ettouney, 2002)

Figure 2.1: Salts composition in Seawater categorised by Mass Concentration

The salinity of seawater varies for specific regions around the world; however, the percentage composition is rather constant (Wang et al., 2011). Seawater composition include considerable quantities of minerals that are a function of partly their contamination by waste discharge, geographic location and contamination containing organic carbon and microbial contaminants among other factors (Micale et al., 2009; El-Dessouky and Ettouney, 2002). Evidently, special technologies will be mandatory to convert the waters into potable water that would be desirable and safe for human consumption and industrial use.

2.2 Desalination Technologies

Desalination technologies separate dissolved minerals and other materials from fresh water. The process technologies can be classified in many different categories, i.e. energy based, mechanisms and separation process adopted. Table 2.2 shows the different kinds of desalination classification.

Irrespective of the technology used, all processes convert the feed water into two streams: a concentrated by product called brine and fresh water containing low level of dissolved salts.

The most common desalination technologies, which accounts for approximately 93%, (Agostinho, 2013; Wang et al., 2011; Micale et al., 2009) used are Multistage Flash Distillation (MSF), Multi-Effect Distillation (MED) and Reverse Osmosis (RO).

Table 2.2: Desalination Classification

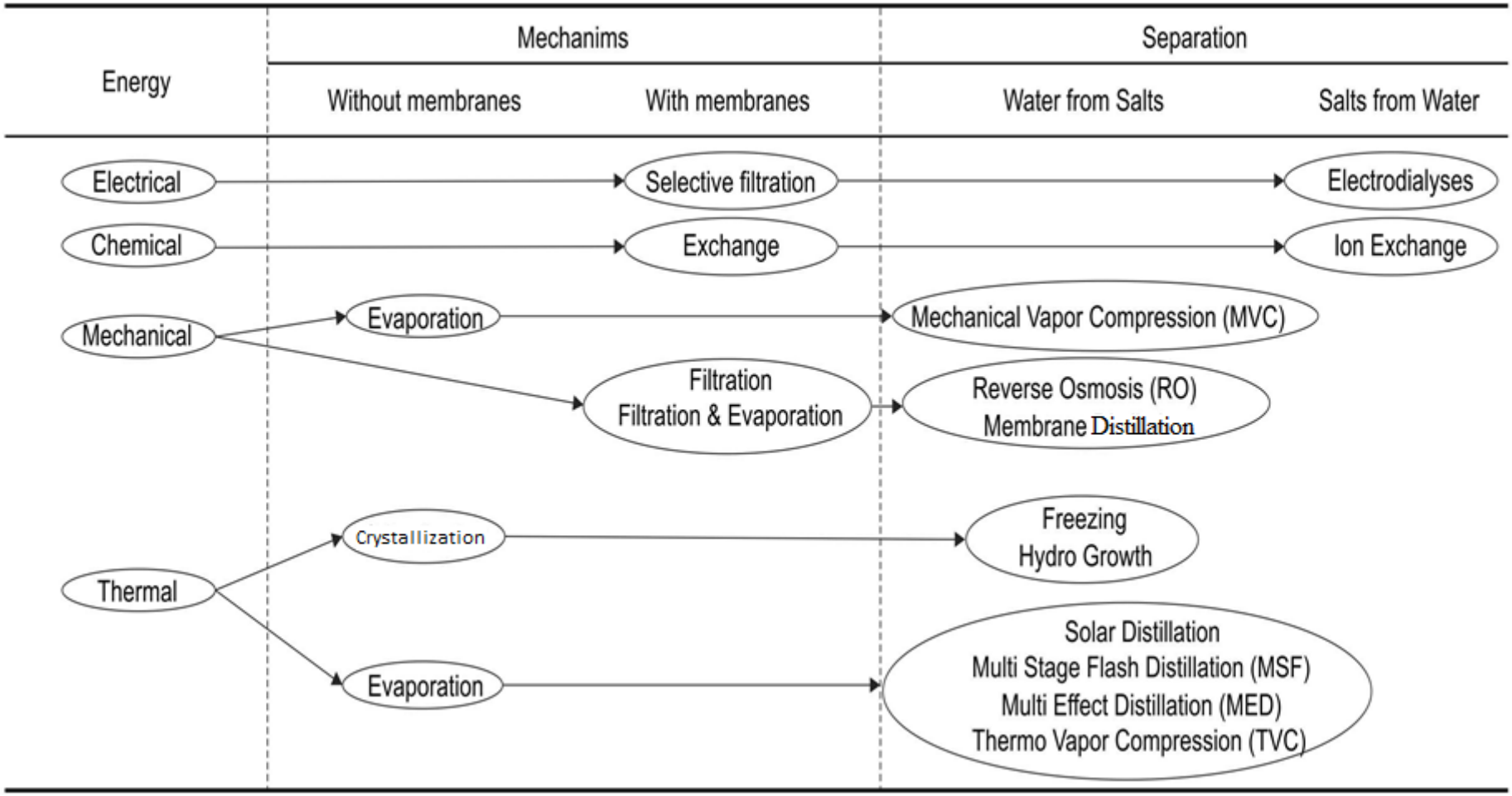

Adopted from (Agostinho, 2013)

The following section describes briefly the most important desalination processes.

2.2.1 Reverse Osmosis (RO)

Reverse osmosis occur when high pressure is used to permeate fresh water through semi-permeable membranes leaving behind a highly concentrated brine solution (Wang et al., 2011; Ettouney and Wilf, 2009; Micale et al., 2009; El-Dessouky and Ettouney, 2002).

In direct osmosis, when liquids with high solute concentration and low solute concentration are separated with a semi permeable membrane, solvent moves to the high solute concentration until there is equal solvent to solute concentration in both sides of the liquid (Figure 2.2 a). Reverse osmosis occurs when pressure causes solvent only to move through semi-permeable membranes leaving a concentrated brine solution (Figure 2.2 b).

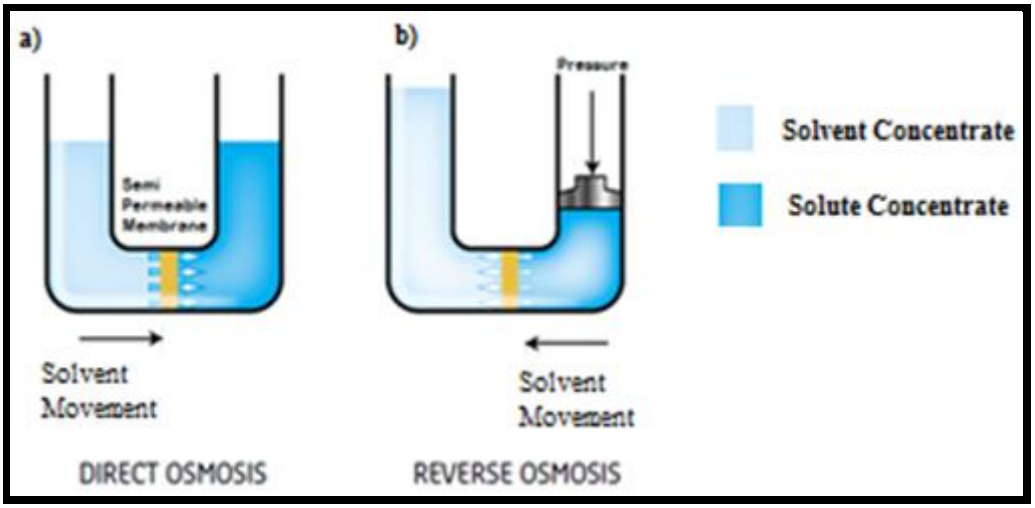

Adopted from (Degremont, 2014)

Figure 2.2: Reverse Osmosis

The membranes used for reverse osmosis are semi-permeable in nature; the separation takes place through a dense polymer layer of microscopic thickness. Pre-treatment is done to the feed water to protect the membranes by controlling microbial growth on the membrane, removing some contaminants and to facilitate membrane operation. (Wang et al., 2011; Ettouney and Wilf, 2009; Micale et al., 2009; El-Dessouky and Ettouney, 2002).

The major drawbacks of this system are that it has high-energy requirement, pre-treatment of the feed water is needed, fouling, breaking of the membrane and high costs of equipment (Wang et al., 2011; El-Dessouky and Ettouney, 2002).

2.2.2 Multi Stage Flash (MSF) Distillation

The Multi Stage Flash (MSF) distillation process is a technique whereby the preheated feed water (Heating Section) boils rapidly and change into steam (flashing effect) when introduced to a chamber with a lower pressure (Flashing Section) as illustrated in figure 2.3 (1st Stage). The steam generated then condenses on the surface of the tubes that are in contact with feed water. That steam thus heats the feed water prior to its flash chamber introduction. This recovers almost all of the heat of vaporization (Heat Recovery Section). The pressure in a following stage has to be lower than the pressure in the previous stage ($P_1>P_2>P_3$) because the temperature of feed water drops by a certain percentage in every stage. Since the evaporation of the water occurs at a low pressure and low temperature, the entire process has low scaling problems. The fresh water is collected in each stage as illustrated in figure 2.3 (Wang et al., 2011; Ettouney and Wilf, 2009; Micale et al., 2009; El-Dessouky and Ettouney, 2002).

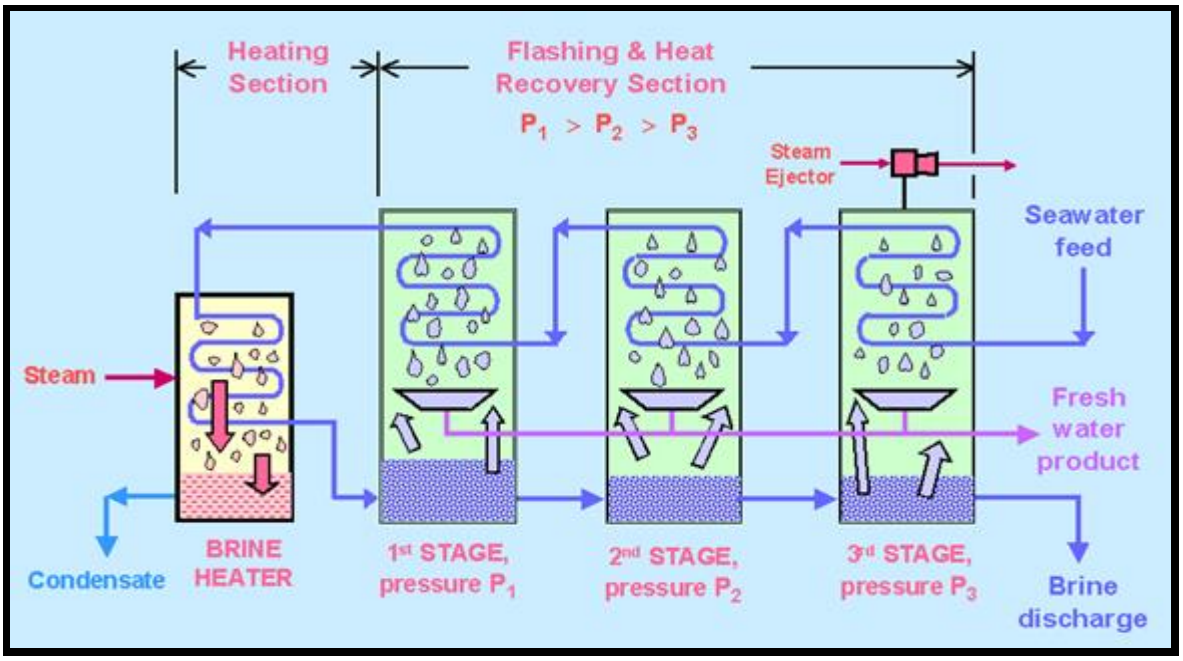

Adopted from (Processes, 2014b)

Figure 2.3: Multi Stage Flash Distillation

Characteristics of MSF plants include scaling and corrosion in the plant, high feed water flow and volume and high rates of treatment chemicals use (Wang et al., 2011; Ettouney and Wilf, 2009; Micale et al., 2009; El-Dessouky and Ettouney, 2002).

The major drawback of this system is that it is an energy intensive process.

2.2.3 Multi-Effect Distillation (MED)

The multiple effect distillation system is formed by a sequence of single effect evaporators. In a single effect evaporator, liquid is atomized on top of a heating tube bundle where it evaporates while brine flows down the tubes and is collected as the by-product (Figure 2.4). The heating tube bundles are heated with either hot water or steam. The vapour, which results from evaporation of the liquid by the heating tube bundles, is then collected and condensed into fresh water, the distillate (Figure 2.5).

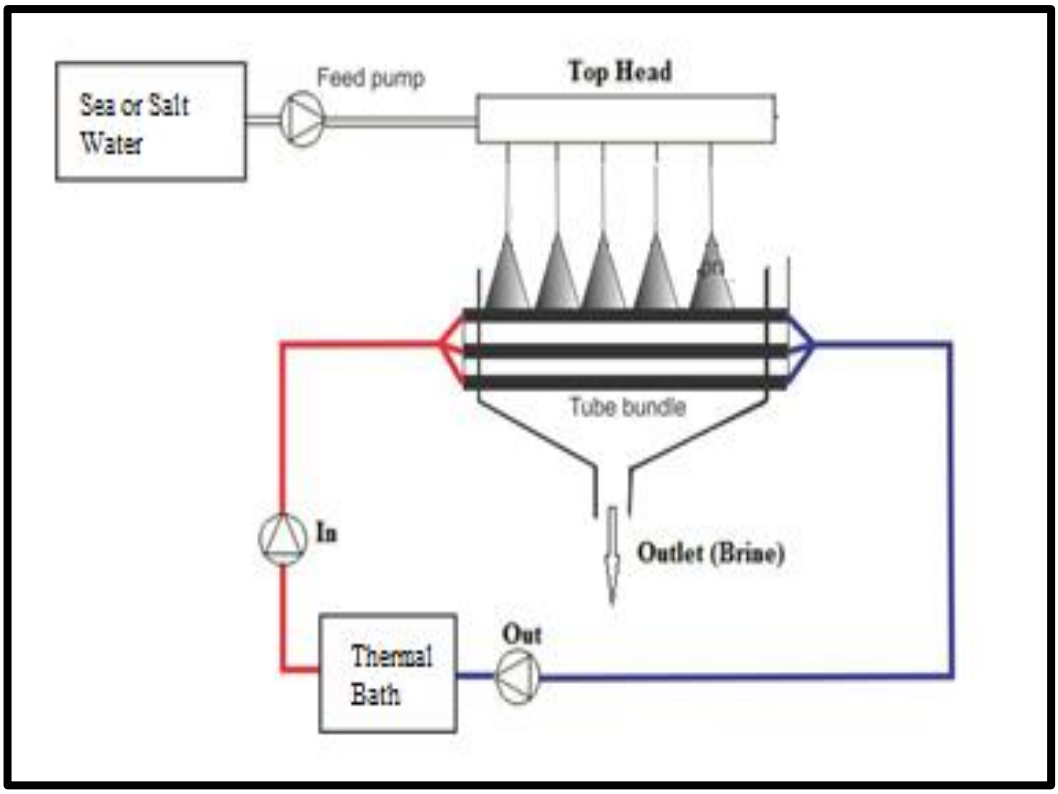

Figure 2.4: Open Configuration of a Single Effect Distillation

Multi effect distillation involves feed water being atomized onto heated tubes inside a series of closed chambers. Evaporation of feed liquid occurs on the outer tube surface while steam condenses on the inner heated tube bundle surface. The formed steam in one effect is subsequently used in the next effect as illustrated by figure 2.5. The reuse of the steam in this system allows for brine reduction. Pressure is reduced successively in each effect ($P_1>P_2>P_3$) and as decrease in temperature is experienced, provision of additional heat is done to improve performance in each stage (El-Dessouky and Ettouney, 2002; Ettouney and Wilf, 2009; Micale et al., 2009). Configurations of MED plants include horizontal or vertical tubes (Wang et al., 2011; Ettouney and Wilf, 2009; Micale et al., 2009; El-Dessouky and Ettouney, 2002). A drawback of this system is that it has a high-energy requirement.

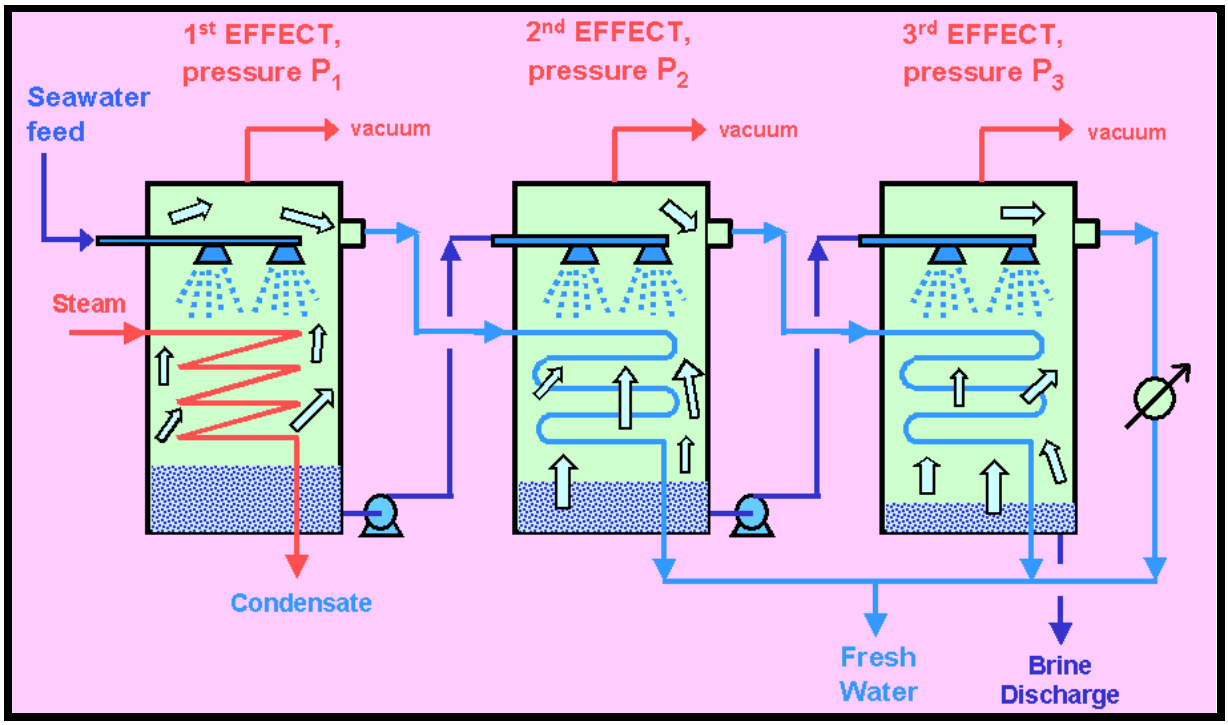

Adopted from (Processes, 2014)

Figure 2.5: Multi-Effect Distillation

2.3 Energy Consumption

The theoretical minimum amount of energy required to separate salt from seawater is 0.7 kWh m^{-3} (Micale et al., 2009). Comparing the amount of energy needed for current processes to this theoretical minimum shows the inefficiency of these processes (Table 2.3). Average electrical energy equivalent is the amount of energy used in preparation of seawater before it is injected to the desalination process per unit output of desalinated water while electrical consumption is the exact amount of energy used in the desalination process for the corresponding process per unit output of desalinated water. Total electrical energy equivalent is the summation of the energy used in the preparation stage and the energy used in the desalination process per unit output of desalinated water. Comparisons have shown that MED is more energy efficient than other thermal desalination processes (Ettouney and Wilf, 2009).

Table 2.3: Energy Consumption for different desalination processes

Process/Energy type	Minimum (Ideal)	R.O	MED	MSF
Average electrical energy equivalent (kWh/m^3)			4.5	14.0
Electrical consumption (kWh/m^3)		3.5 - 5.0	1.2 - 2.0	3.0 - 4.0
Total electrical energy equivalent, (kWh/m^3)	0.7	3.5 - 5.0	5.7 - 6.5	17.0 - 18.0

Adapted from (Ettouney and Wilf, 2009)

Having compared the major desalination technologies currently in use in the market, it is concluded that they fall short of producing fresh water using techniques that have low energy requirement. Therefore, there is a gap left to be filled and the intended development is combination of the above processes with electrohydrodynamic atomization (EDHA) to optimise the process.

2.4 Electrohydrodynamic Atomization (EDHA)

2.4.1 Atomization

Atomization is the disintegration of a liquid into small droplets (Ashgriz and Yarin, 2011). The formation of a droplet is the result of different forces overcoming the surface tension of the liquid. There are many different atomization mechanisms. These processes are mainly classified by the energy type used to breakup the liquid. The most common types are: Electrohydrodynamic atomizers, rotary atomizers, ultrasonic atomizers and pressure atomizers.

Atomization of a liquid occurs when liquid is pumped through a nozzle and through different regimes due to the difference in flow rate and nozzle geometry. A regime is defined as the different droplet formation process which is as a result of the different flow rate when a pumped liquid goes through a nozzle and there is no applied electric potential. Clanet and Lasheras (1999) characterised the different regimes when different flow rates are pumped through a nozzle. When liquid is pumped with a low flow rate, it forms a convex meniscus which grows in size over time to a pendant shaped droplet which detaches itself and the cycle starts all over again. This is called the dripping regime (Figure 2.6 (a)). In the jetting regime, the liquid will form a jet when liquid is pumped at a higher flow rate and the droplets will be formed from the breakup of this jet. The jetting regime is illustrated in figure 2.6 (c). The regime that is between (a) and (c) is called the dripping faucet or transition regime (Figure 2.6 (b)).

The transition between the regimes depends basically on the flow rate of the liquid but it is also influenced by the nozzle geometry and the liquid properties namely: velocity, density and surface tension (Clanet and Lasheras, 1999). The different regimes can be expressed in relation to the liquid Weber number (We) where the liquid weber number is expressed in equation 2.4.1 (Clanet and Lasheras, 1999).

$$We = \frac{\rho_l r v^2}{\gamma} \quad \ldots\ldots\ldots\ldots\ldots\ldots\ldots\ldots\ldots\ldots\ldots\ldots\ldots\ldots\ldots\ldots \mathbf{2.4.1}$$

where r is the nozzle inner radius (m), ρ is the liquid density (kg/m^3), ν is the velocity of the liquid through the nozzle (m/s) and γ is the surface tension of liquid (N/m).

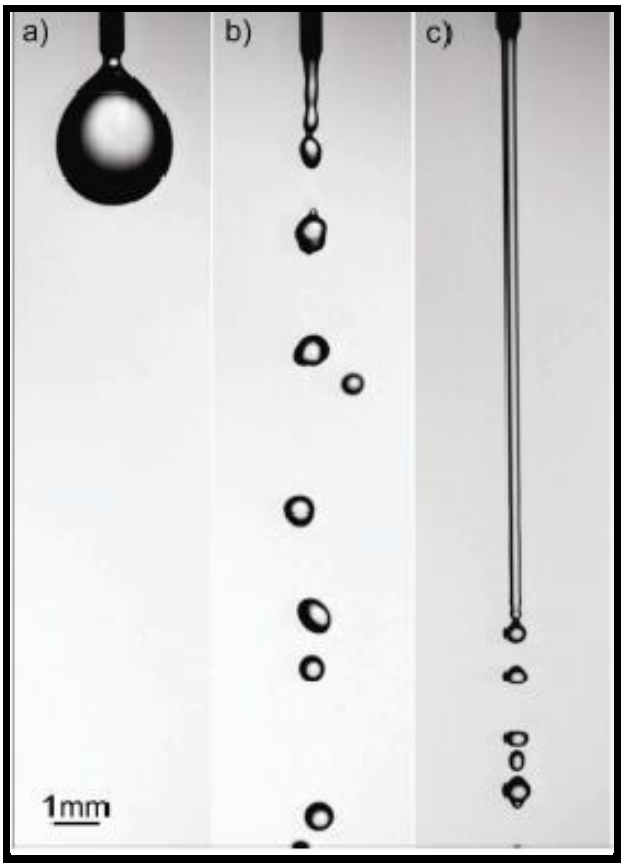

Adopted from (Agostinho, 2013)

Figure 2.6: Droplet Formation Mechanisms. (a) is dripping regime, (b) transition or dripping faucet regime and (c) jetting regime.

Using the dimensionless weber number value (Equation 2.4.1), the dripping regime occurs at We < 2.5, the dripping faucet regime at 2.5 < We < 4 and the jetting regime takes place at We > 4 (Agostinho, 2013; Van-Hoeve et al., 2010).

Since electrohydrodynamic atomization has the possibility of controlling the droplet diameter, the charge of the droplet and the dispersion of the droplets, therefore, it is a favourable option to be coupled with a desalination technique for efficiency optimization.

2.4.2 Electrohydrodynamic Atomization/Electrospray

Electrohydrodynamic Atomization (EDHA) is the process of liquid breaking up into droplets using electric stresses created by applying a strong electric potential difference. It is commonly referred to as electrospray. In general, the liquid is pumped through a nozzle and the electric potential difference field is applied between a counter electrode and the nozzle placed close to the counter electrode. There are different configurations to achieve the setup but the dominant ones are: (1) Nozzle to plate (Figure 2.7 (a)) and (2) nozzle to ring which is divided into two types: nozzle to ring down (Figure 2.7 (b)) and nozzle to ring up (Figure 2.7 (c)). The advantages of this process are the capability of controlling the droplet diameter and the wide droplet dispersion. Different combinations of flow rate and applied potential can create different sprays for the same liquid through the same nozzle geometry thus it yields the different electrospray modes.

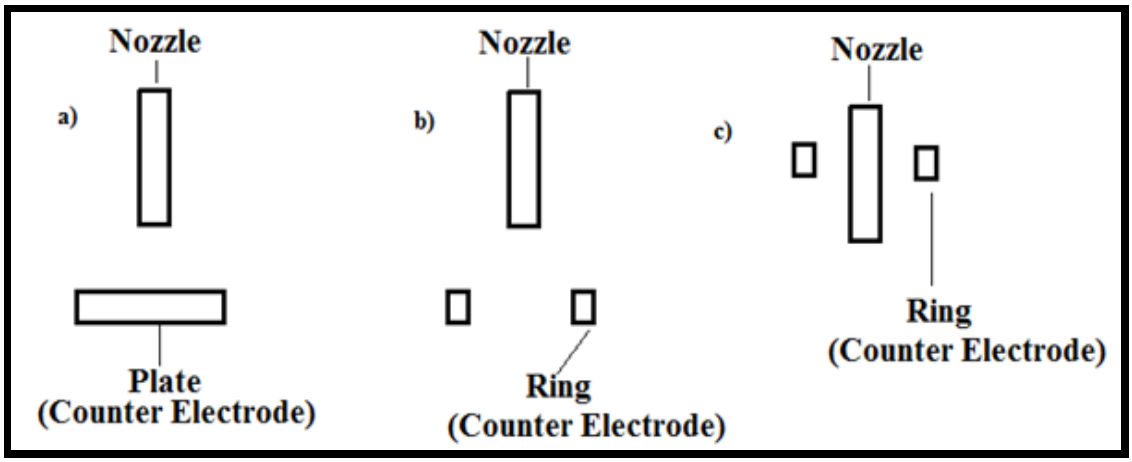

Figure 2.7: Nozzle-Counter Electrode Configurations

2.4.3 Electrospray Modes

Electrospray modes are observed when a change in applied voltage and flow rate for constant liquid properties results in several visual and measurable differences in the droplet formation. These differences are defined as spray modes. Electrospray depends on the intensity of the electric field and the flow rate of the liquid. The electric forces change the force balance on the liquid surface initiating the droplet formation mechanism. Several authors (Jaworek and Krupa, 1999; Grace and Marijnissen, 1994 and Cloupeau and Prunet-Foch, 1994) have classified the modes differently but classification by Agostinho (2013) was adopted for this case (Figure 2.9). However, the classified modes do not apply for all liquids (Grace and Marijnissen, 1994) and they also do not occur in the same chronological order for all liquids (Yurteri et al., 2010).

For low values of the electric potential during the dripping regime, the dripping mode is observed (Figure 2.6). The droplets are bigger than the nozzle diameter when detaching at very low frequencies (Grace and Marijnissen, 1994). With increase in applied voltage, the droplets frequency also dripping increases and the diameter of the droplets decreases (Agostinho, 2013).

When the applied potential is further increased, the intermittent cone-jet mode or the spindle mode occurs (Figure 2.8). Both modes are pulsating that is they are not continuous. For the spindle mode, the cycle starts with an about hemispherical meniscus, which changes into a conical shape and at its apex, a jet forms. This jet breaks up into small droplets. Then the ligament breaks from the cone and further breaks into one big droplet and small droplets while the cone relaxes into an almost flat meniscus (Figure 2.8). The process repeats regularly depending on the applied voltage and flow rate used (Yurteri et al., 2010).

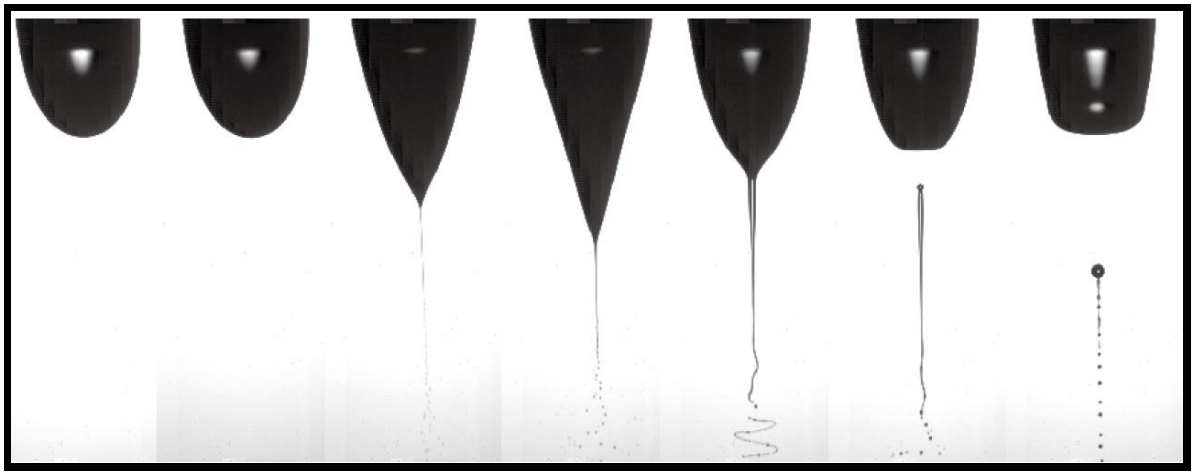

Adopted from (Yurteri et al., 2010)

Figure 2.8: Spindle Mode

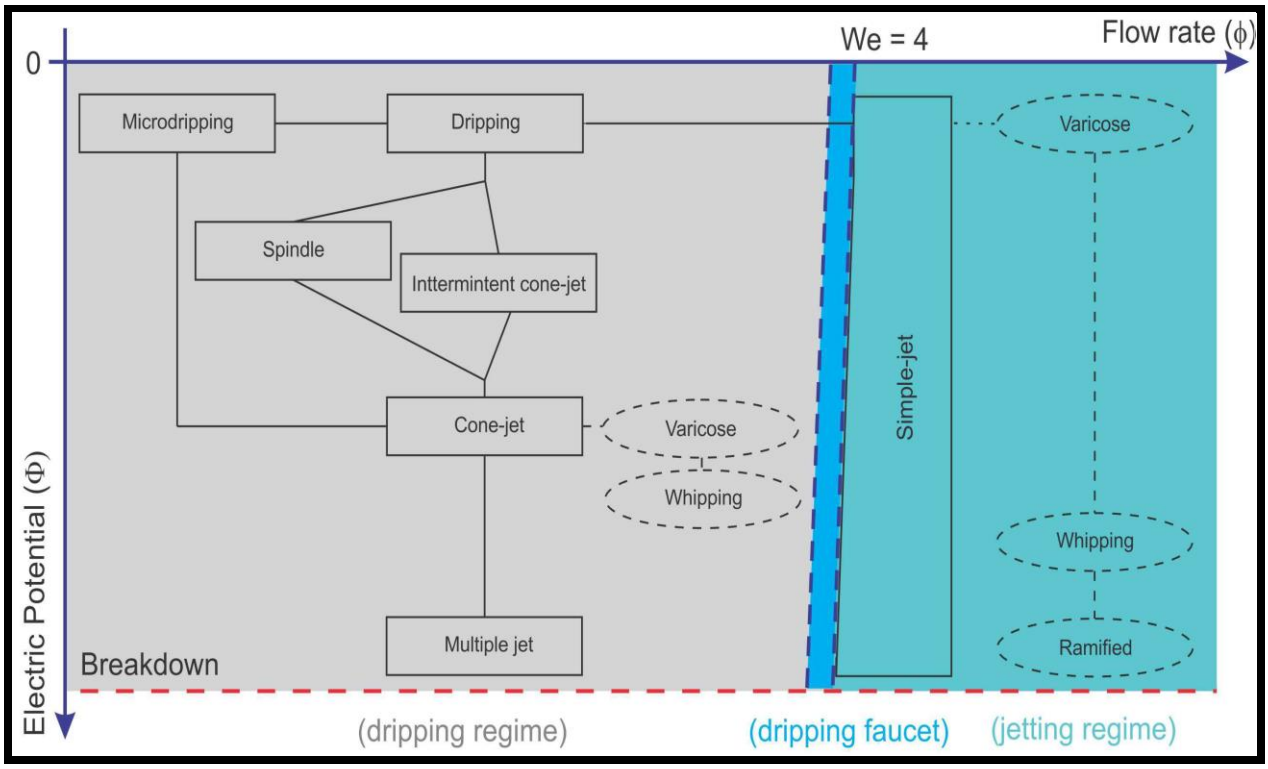

Adopted from (Agostinho, 2013)

Figure 2.9: Electrospray Modes

For intermittent cone-jet mode, the cycle starts with a hemispherical meniscus, followed by the droplet shape changing into a conical shape and at its apex, a jet emerges. The jet breaks up into highly charged droplets that cause space charge which reduces the electric field at the liquid cone (Figure 2.10). This field reduction causes the surface tension to overcome the electrical stresses (Hartman, 1998). The liquid cone finally relaxes to a meniscus and the cycle starts again (Yurteri et al., 2010).

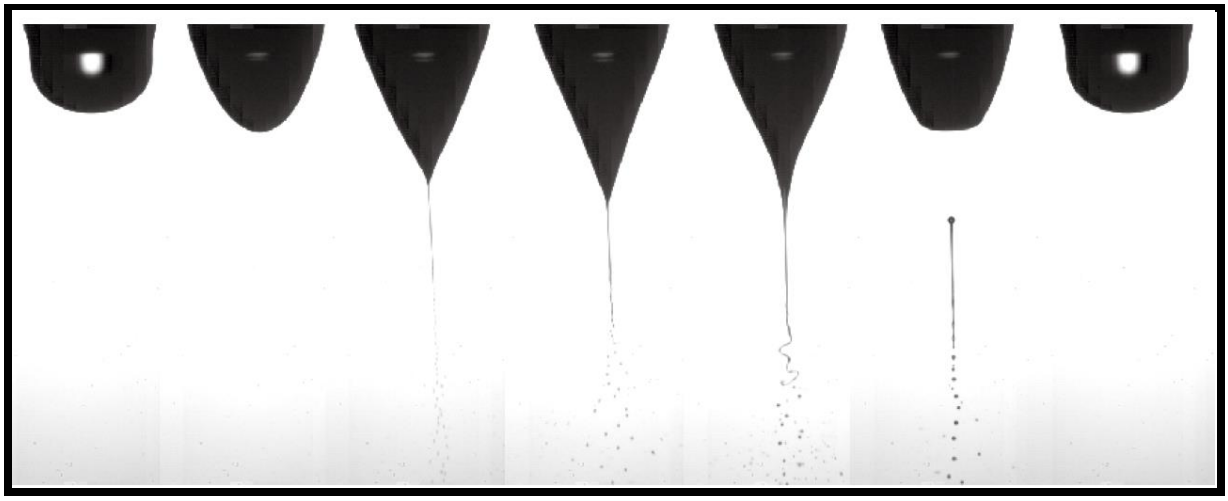

Adopted from (Yurteri et al., 2010)

Figure 2.10: Intermittent cone-jet mode

Further increase in potential while at intermittent cone-jet mode (Figure 2.10), the cone jet mode is realised. The cone jet mode occurs when the meniscus forms a stable cone (conical shape) and a jet emerges from its tip which then breaks up into droplets. This is known as the varicose breakup of the cone jet mode. The formed droplets have a narrow sized Gaussian distribution and are much smaller than the nozzle diameter (Figure 2.11). Inside the same cone-jet window and if the potential is increased, the varicose breakup is influenced by kink instabilities, which is the whipping breakup. For even higher potentials more cone-jets appear and the multiple-jet mode is formed. Figure 2.11 shows the progression of the formation of the stable cone jet mode.

Adopted from (Yurteri et al., 2010)

Figure 2.11: Cone-jet mode

If the electric potential is increased past the multiple-jet mode then the air undergoes an electrical breakdown and sparking is observed (Figure 2.9) (Agostinho, 2013).

2.5 Simple Jet Mode

Simple jet mode occurs when the liquid flow rate is high and the kinetic energy of the liquid is too large to be counterbalanced by the surface tension hence a free jet is formed breaking up into small droplets (Hartman, 1998). According to Agostinho et al., (2012), simple jet mode is defined as a stable and continuous jet mode in which the breakup happens from an electrified jet but at flow rates in the order of the dripping faucet and/or the jetting regime (Figure 2.9).

This mode forms a stable jet continuously and has a relatively high flow rate (Figure 2.12). Since it has a higher flow rate than all the other modes, it will therefore be the most suitable

mode to be used in situations which require high throughputs (Agostinho et al., 2013a) for example water desalination plants and also for irrigation purposes.

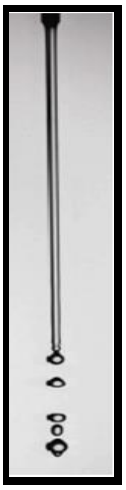

Adopted from (Agostinho, 2013)

Figure 2.12: Simple-jet mode.

2.6 Multinozzle Configurations

Since the desired droplet size is a function of the nozzle inner diameter among other factors, increasing the number of nozzles is the only viable method of increasing the output if the flow rate remains constant. Various multinozzle devices have been developed previously and the most important are explained here.

A multi-hole electrospray atomizer was constructed by Bocanegra et al. (2005), which had a packing density of up to 115 emitters per square centimetre with only 37 holes. It was one of the first multinozzle configuration atomizers, which were constructed. Feeding was done by a pump and it was operated in the cone jet mode. In their report, they concluded that when orifices were drilled in hydrophobic surface dielectric materials, the reliability and stability of the electrospraying process from holes improved substantially.

Deng et al. (2009) demonstrated the successful operation of a multiplexed electrospray system with a packing density of up to 11,547 sources per square centimetre. Feeding was done by a pump while being operated in the cone jet mode. The authors were able to show that the droplets size was uniform across the entire spray region.

A multinozzle system operated with a high precision pump and using a hydraulic head with a packing density of up to 1,964 sources per square metre was designed, constructed and studied by Arnanthigo et al. (2011). Each nozzle was in isolation in a cylindrical injection chamber to minimise spray interference and was fed by a high precision pump. They concluded that the accuracy of the liquid feeding system associated with a high-cost pump is

what determines the stability of particle production from multi-nozzle electrospray systems. A constant head feeding mode was also proposed and a semi-empirical model was developed to predict the flow rate in that configuration.

Agostinho (2013), Agostinho et al., (2013b) and Brouwer (2011) designed, developed and studied a 5 nozzle electrospray device operating in the simple-jet mode with an insulating layer placed between the ring counter electrode plate and nozzle tips. It had a packing density of up to 1,228 sources per square metre and was fed by a pump. The authors concluded that when the additional insulating layer was placed between the counter electrodes and the nozzle tips, the multinozzle device was able to operate inside closed chambers with high humidity levels without current leakages.

Yurteri, et al. (2010) reviewed the multinozzle devices and concluded that electrical interferences between the neighbouring sprays and variation in liquid flow rate to all nozzles are challenges that should be overcome while designing a multinozzle device. This conclusion was shared also by other authors like (Agostinho, 2013; Agostinho et al., 2013b; Brouwer, 2011).

2.7 Liquid Analysis Instrumentation

Inductively Coupled Plasma Mass Spectrometry (ICP-MS) and Total Reflection X-ray Fluorescence (TXRF) analytical equipment were used for liquid analyses.

Inductively Coupled Plasma Mass Spectrometry (ICP-MS) is a destructive testing analytical equipment which can analyse a wide range of elements in the periodic table and especially well for low Z elements, for example B, Li, Na and Mg (Wang et al., 2000). It has detection limits of less than one part per trillion (10^{12}) (ppt) for many elements in the periodic table, isotopic analysis is readily achievable and productivity that cannot be outshined by any other analytical technique (Voica et al., 2012).

Total Reflection X-ray Fluorescence (TXRF) is a non-destructive testing analytical equipment with detection limits in the order of parts per billion (10^{9}) (ppb). It involves the total reflection of the incident X-rays used to excite a sample. The incident and reflected beams have the same energy and intensity. TXRF uses small quantities of liquids for its analysis (Klockenkämper, 1997).

3. METHODOLOGY

3.1 Single Effect Chamber

To get acquainted with the electrospray technique as well as understand the multinozzle systems, experiments were performed using an existing 10 nozzle atomizer system coupled with a single effect chamber measuring 640 mm length, 390 mm width and 490 mm height as seen in figure 3.1. This was instrumental in identifying the strength and weaknesses of the system, giving insights of how to design a better multinozzle atomizer and understand the working of the complete system.

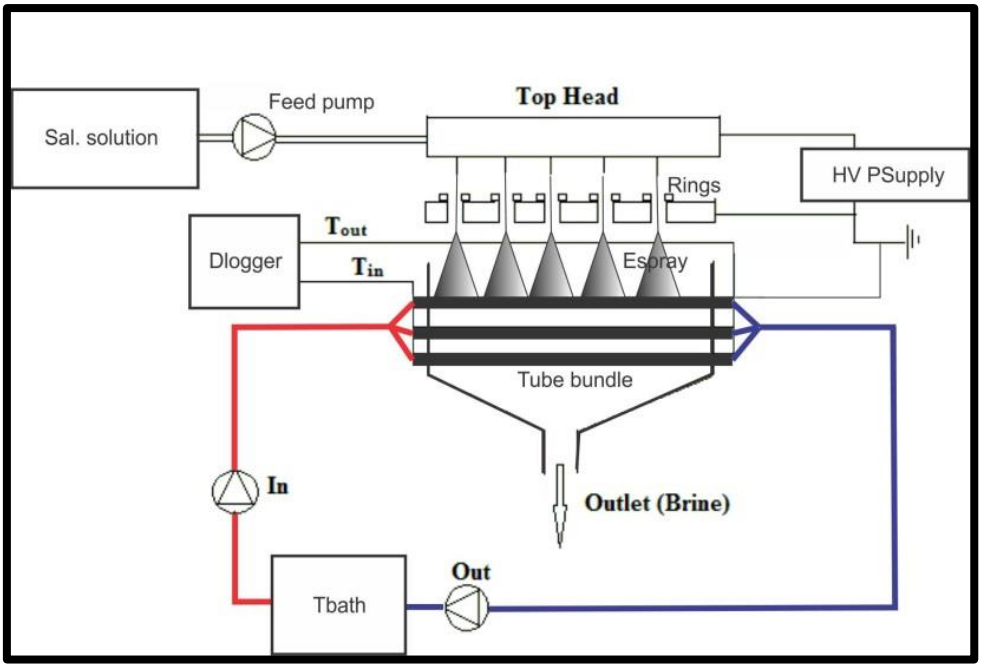

Figure 3.1: Schematic Diagram of the 10 Nozzle Atomizer coupled with a Single Effect Chamber

A high voltage supply was used to provide the potential difference between the nozzles and the counter electrodes (rings) (Figure 3.2 (a)). The high voltage was connected to the tubular multinozzle while the counter electrodes and the evaporation tube bundles were grounded. The tubular multinozzle consisting of 10 nozzles equidistant from each other, five nozzles on each top head tube, were connected to a source of water. Water, at room temperature (23ºC), was pumped using a Simdos Fem 1.10 pump at a constant rate of 5 L h^{-1} which results to a flow rate of 0.5 L h^{-1} per nozzle (Figure 3.2 (a)).

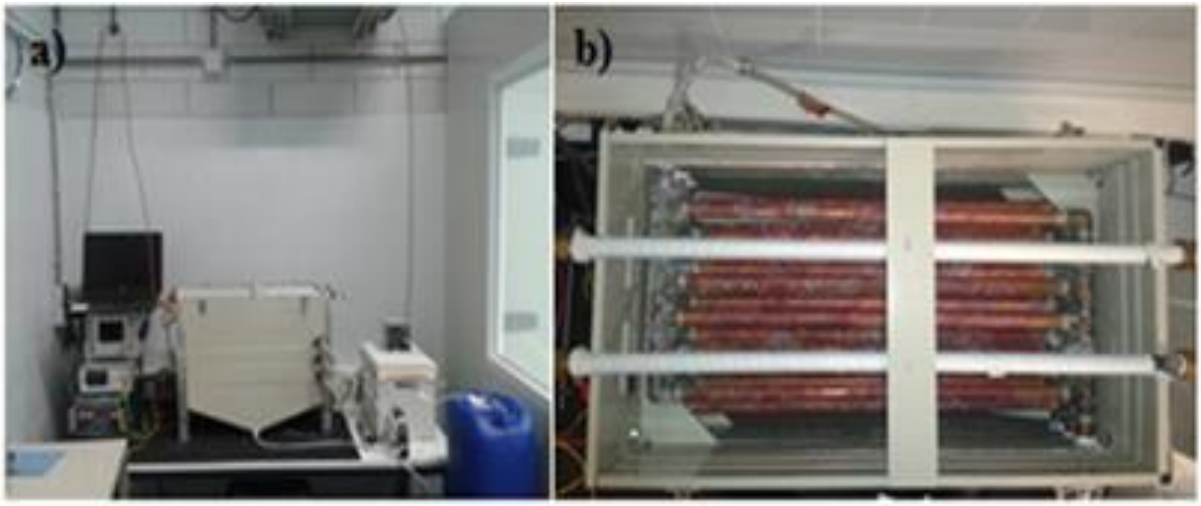

Figure 3.2 (a and b): Single Effect Chamber. (a) Laboratory Chamber Setup (b) Evaporation Tube Bundles.

The evaporation tube bundles of outer diameter of 22 mm had three levels (Figure 3.1 and 3.2 (a)). Water was heated and pumped throughout the tube bundle until the temperature stabilized (77ºC) after two hours. The water running through the tubes and the water bath formed a closed loop. Temperature sensors (PT 100) were fitted to both the inlet and outlet at each tube level in order to measure the temperature difference which was used to calculate the heat used to evaporate the atomised water. All of the temperature sensors were connected to a data logger (Endress Hausser RSG30) to allow for visual determination of the temperature in real time. The electrosprayed water was partly evaporated when the droplets fell on the surface of the heated evaporation tube bundles. The evaporation tube bundles were grounded to prevent the data logger from being affected by the charges in the droplets (Figure 3.2 (a)). The experiment was conducted in an open configuration in which the lid was removed from covering the reactor body. The single step chamber was also grounded to prevent accumulation of charges in the chamber body (Figure 3.2 (a)).

Five experiments under the same conditions were performed for different values of potential difference (0 kV, 2 kV, 4 kV, 6 kV and 7 kV). For each voltage, the temperature of the evaporation tube bundles, at all the three levels, for both the inlet and outlet, was measured and recorded.

3.2 Droplets Attraction to Tube Experiments

The main objective of electrospray in this project was to create disperse droplets so as to increase the surface area for evaporation. Once atomization by the electrospray process has occurred, the sprayed droplets should be attracted onto an evaporation surface for increased evaporation to occur in thermal desalination processes. Therefore, more experiments were necessary to investigate the distance the evaporation surface should be placed and the required voltage to be used to avoid interference of the electrospray electric field.

Bench scale experiments of a single nozzle electrospray set-up were developed and done in order to determine the required potential and the appropriate distance needed to attract the charged droplets to the evaporation tube without affecting the electric field causing electrospray. A copper tube was used as an evaporation surface during the experiments to simulate the real conditions in a multi effect distillation process. To investigate this, two different configuration were used. Figure 3.6 (a) and (b) shows a schematic diagram of the bench scale setups.

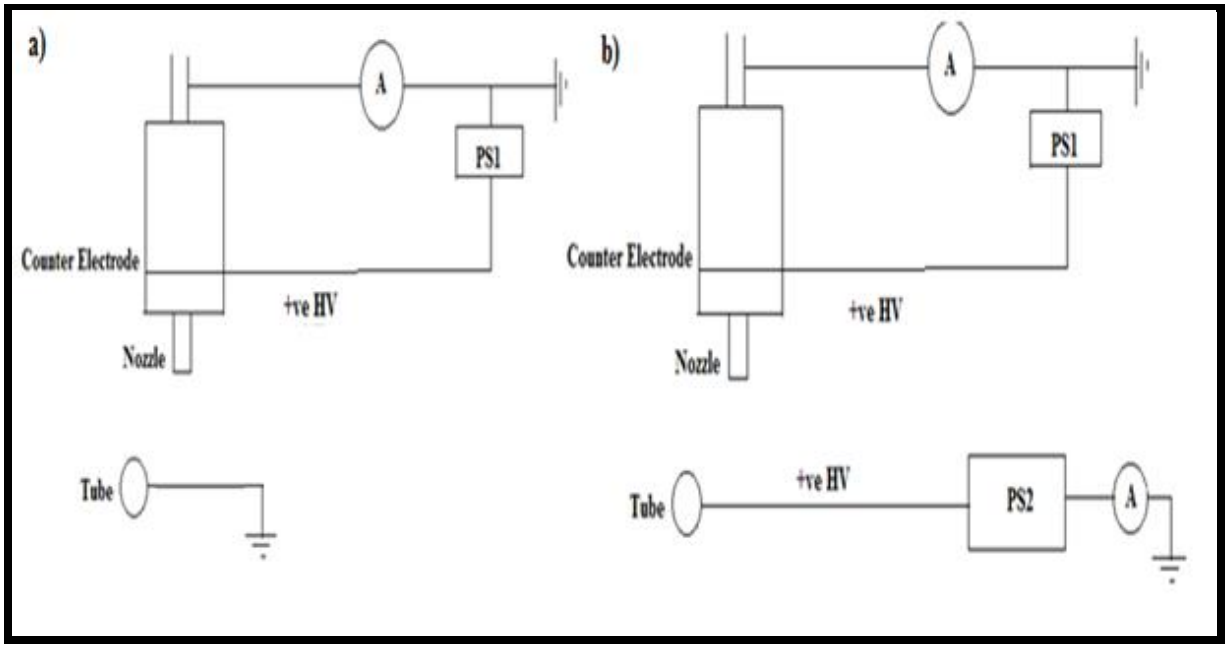

Figure 3.3: Schematic Diagram of the Set up with grounded tube (a) with charged tube (b)

Setup 3.3 (a) was used to verify whether a grounded tube could be used to attract the charged droplets of deionized water at different distances. In this setup, a power supply (PS1) was used to produce the electrospray while the copper tube was grounded. A tube, 22 mm outer diameter and 160 mm length as shown in figure 3.6 (a), was offset to the left by 20 mm from the axis of the spray nozzle. In this experiment, different distances (20, 40, 60, 80, 100, 200

and 300 mm) of the copper tube from the nozzle tip to the tube surface were investigated while kept grounded. The nozzle used for the experiments was an EFD precision nozzle tip, gauge 22 with 0.71 mm outer diameter, 0.41 mm inner diameter and 25.4 mm long. The electrospray was generated by the PS1 using a constant flow rate (500 mL h^{-1}), grounded nozzle and charged ring at constant potential (4 kV). The electrospray configuration used was nozzle to ring up. The distance between ring and nozzle tip was also kept constant at 17 mm.

A charged tube was used to verify whether there was attraction of the droplets of deionized water at different distances as illustrated by setup 3.3 (b). For this experiment, two power supplies were used; the first power supply (PS1) to produce the electrospray and the second power supply (PS2) to charge the copper tube. A tube, 22 mm outer diameter and 160 mm length was offset to the left by 20 mm from the axis of the spray nozzle. The distance of the copper tube surface to the nozzle tip was varied (20, 40, 60, 80, 100, 200 and 300 mm). The potential on the tube was increased to check the minimum value which would provide attraction of the droplets for each tested distance. The first power supply generated the electrospray using a grounded EFD precision nozzle tip, gauge 22 with 0.71 mm outer diameter, 0.41 mm inner diameter and 25.4 mm long nozzle, a charged ring at a fixed potential (4 kV) and at a constant flow rate (500 mL h^{-1}). The distance between ring and nozzle tip was also kept constant at 17 mm.

Photographs of the attraction of the droplets to the tube were taken using a Canon EOS 70D digital camera at long exposure times of about 0.5 second when front illumination was provided for.

3.3 Multinozzle Design Study

The design concept of the prototype of a multinozzle atomizer was arrived by combining the conclusions and recommendations of the single effect chamber experiments and the droplets attractions to tube experiments as well as evaluating studies by Geerse (2003) and Agostinho et al., (2013). The concept was drawn using SolidWorks® engineering software. Thereafter, modelling using Comsol® Multiphysics Software was done. This was done to predict the expected electric field of the proposed set-up and to track the particle in the electric field thus giving a prediction of the dispersion expected in the actual running of the set-up. The results obtained from the experiments using the prototype, a multinozzle atomizer concept was drawn and modelled.

A flow chart of the processes involved was drawn (Figure 3.4).

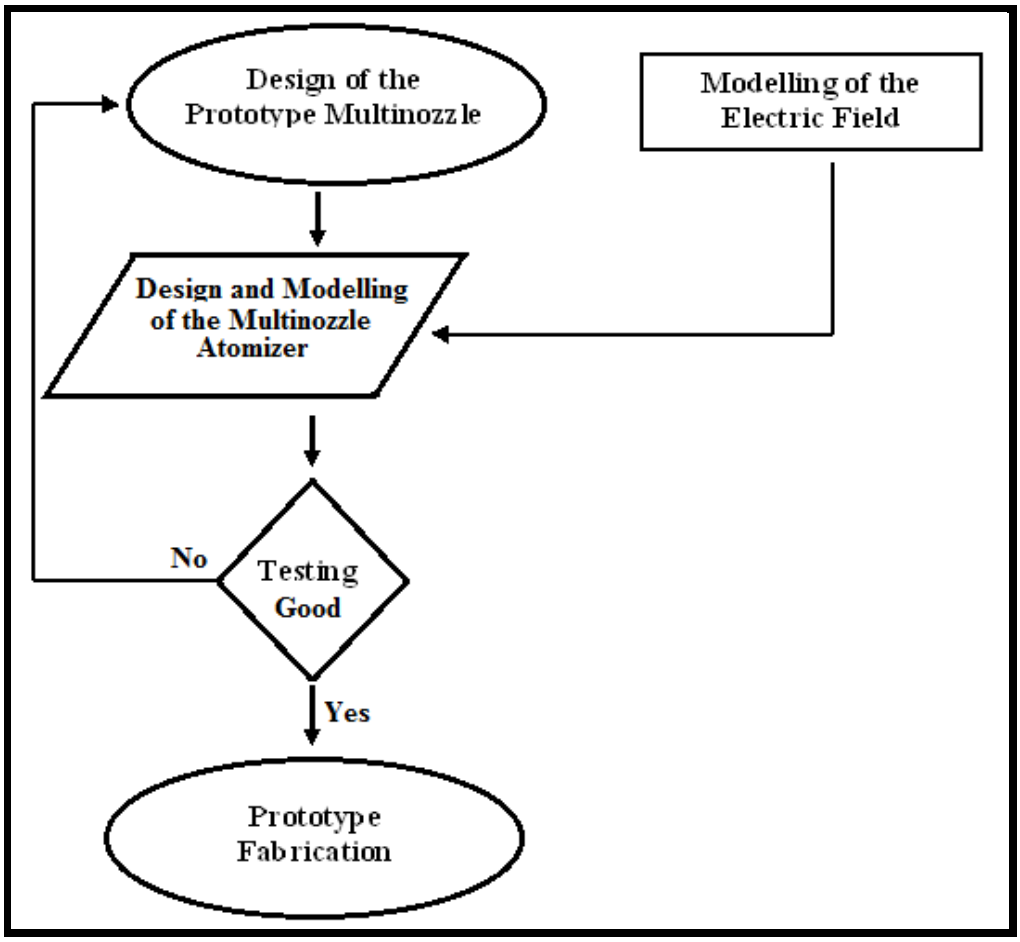

Figure 3.4: Flow chart of the development process

3.4 Prototype Design

The design arrived at had 22 nozzles and an insulated ring-up (counter electrode) configuration (Figure 3.5). It was chosen because it provided a dense configuration within the available area without disturbing the electric field of the individual nozzle as well as it prevented short circuiting of the nozzle and counter electrode during operation. The packing density of this configuration was found to be $2.2*10^3$ nozzles m^{-2} compared to $1.2*10^3$ nozzles m^{-2} packing density used by Agostinho (2013). The largest readily available circuit board within budget constraints was 100mm by 100mm. The electrospray configuration used was nozzle to ring-up to allow easy manipulation of the droplets at a later stage.

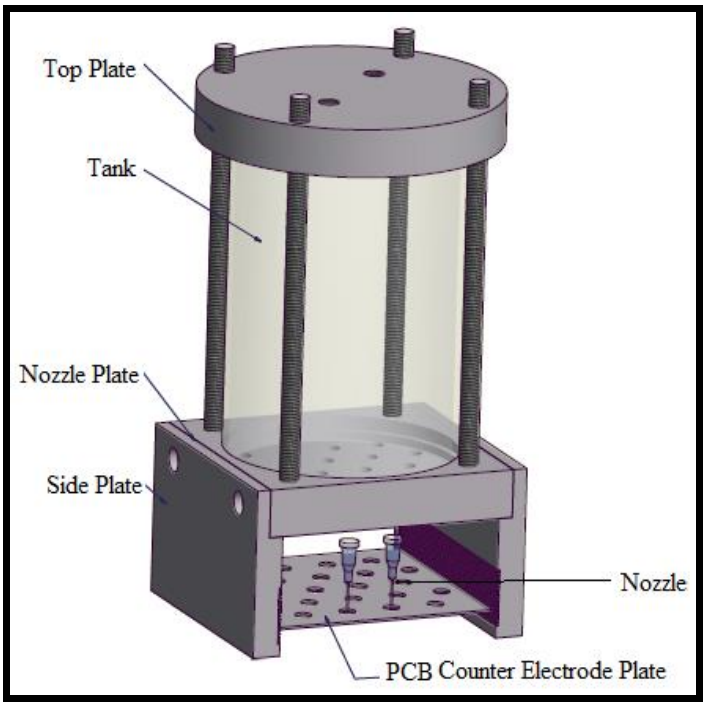

Figure 3.5: Schematic Drawing of Prototype Design

A nozzle and ring- up electrospray configuration with the nozzles grounded and the counter electrodes (rings) charged was used for the experiments. The device was composed of 22 nozzles arranged in an alternating array of 4 nozzles in each array and 5 nozzles in the alternating array. The 4 nozzles array is replicated three times while the 5 nozzles array is replicated two times. All nozzles are equidistant to each other. A 20 mm outer diameter and 15 mm inner diameter counter electrode (rings) were used. The configuration was chosen for its compactness.

The counter electrodes are copper rings embedded in an insulation layer, positioned concentrically with each nozzle and placed 17 mm above the nozzle tip as proposed by Geerse (2003). An insulation layer made of circuit board was used to avoid the possible contact between the nozzles and the rings due to satellite droplets and vapour depositions which would short circuit the system during operation. This proved to be a very efficient way when performing experiments when coupled with the evaporation chamber (Agostinho et al., 2013b).

The body of the multinozzle device was made of Polyoxymethylene because it has high chemical and corrosion resistance, high tensile strength, excellent dielectric properties and low moisture absorption. The tank was made of glass to allow visualization of the liquid to gas interface. For detailed drawing of the components (See appendix B Figures 7.1 to 7.6).

3.5 Bench Scale Experiments

Experiments were carried out to investigate the behaviour of the electrohydrodynamic multinozzle atomizer regarding the following main parameters: electrosprayed droplets size as a function of the inner nozzle diameter and voltage, droplets size distribution, dispersion symmetry of the droplets and electric field for different applied voltages.

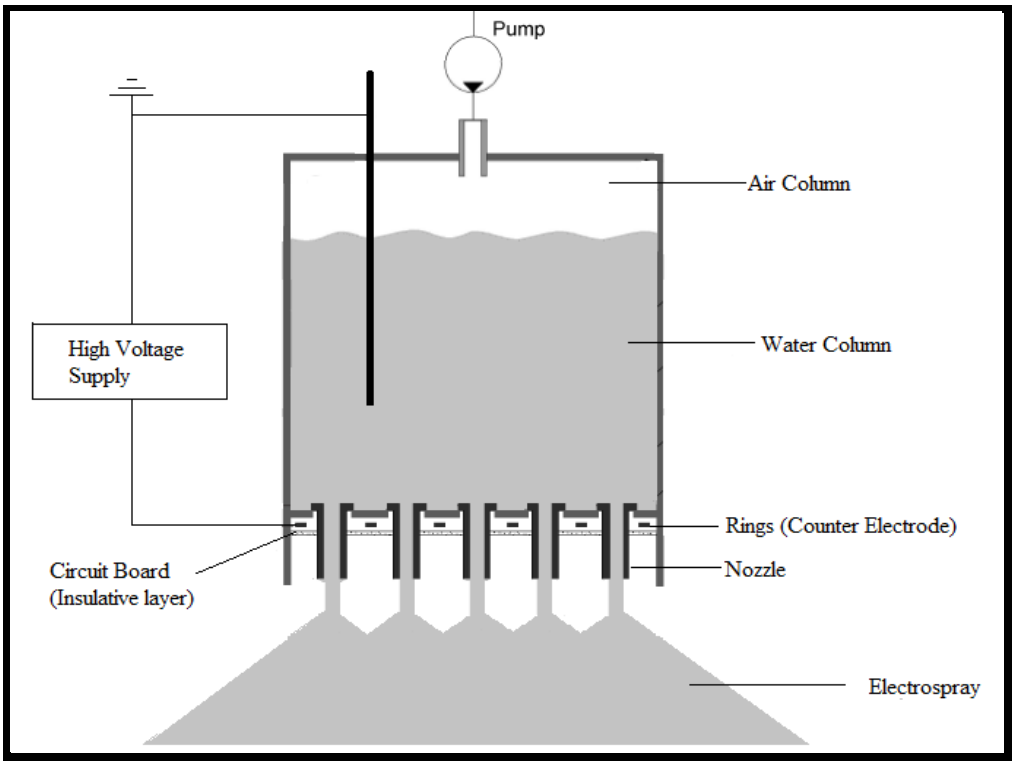

Figure 3.6: Schematic Diagram of the Multinozzle Atomizer

A high voltage supply, FUG HCP 35-35000 DC power supply, was used to provide the potential difference between the nozzles and the counter electrodes (rings) as seen in figure 3.6. The liquid was pumped through an aperture on the top part of the chamber using a pump (Masterflex L/S standard digital drive and the mounted head was a Masterflex L/S Easy-Load II Head for Precision Tubing, PPS/SS EW-77200-60). To maintain a constant and equal flow rate through each nozzle and decrease possible oscillations from the pump, an air column was kept above the liquid/gas interface inside the chamber (Figure 3.6). This tank got pressurized due to the action of the pump. The nozzles used for the experiments were EFD precision nozzle tips, gauge 22 with 0.71 mm outer diameter, 0.41 mm inner diameter and 25.4 mm long. This gives a packing density of 2.2* nozzles m^{-2}. The copper rings acting as counter electrodes were positioned concentric to each nozzle and placed 17 mm above the nozzle tip.

The experiments were done for three different flow rates (360, 420 and 500 mL h^{-1}) which were within the simple jet mode and for each flow the potential applied was varied. The experiments were performed at room temperature and pressure conditions. The liquid used for the experiments was seawater. Seawater was chosen to ascertain the effect of application of high voltage on a liquid with high elemental concentration.

This multinozzle prototype in the simple jet mode was found to have a higher liquid output of 11 L h^{-1} compared to 2.2 L h^{-1} used by Agostinho et al., (2012) and since simple jet mode is less explored; this is the highest reported flow rate to be done. Additionally, the packing density almost doubled from $1.2*10^3$ to $2.2*10^3$ nozzles m^{-2}.

3.6 Droplets Properties

The stability of the spray at each nozzle was investigated by measuring the droplet size at each nozzle using high speed imaging (Timebench® Camera CR 450*3). In each measurement, 438 images were recorded at 1000 frames per second. The measurement was repeated for each nozzle individually. The droplets sizes were analysed using Image J® and Microscoft Excel® package was used to calculate the frequency distribution of the droplets.

Spray symmetry and dispersion were also investigated. Photographs of the spray were taken 1.5 metres away using a Canon EOS 70D digital camera using long exposure times of about 0.5 second when back illumination was provided for.

3.7 Electric Field Modelling

To understand the electric field and particle trajectories to be taken by the droplets, modelling of the whole set-up was done. Comsol® Multiphysics version 4.4 was used to model the characteristics of the electric fields. Modelling of the electric field involved predicting of the electric field without the presence of the liquid.

It was done with the Electrostatic group of equations inside the 3D AC/DC module. The Electrostatics module allows for electric potentials, charges and grounds to be applied to different geometrical objects. Comsol material library was used to define the physical properties of the modelled objects. The counter electrode material was defined as copper; the nozzle as stainless steel, insulation board as FR-4 (circuit board) and the surrounding material inside the box was set as air (Figure 3.7).

The boundaries conditions were defined as follows: The rings boundaries were defined with an electric potential of 6 kV. The nozzles boundaries were defined as grounded. The board

boundaries were selected as dielectric shielding and the surroundings boundaries were selected as no charge.

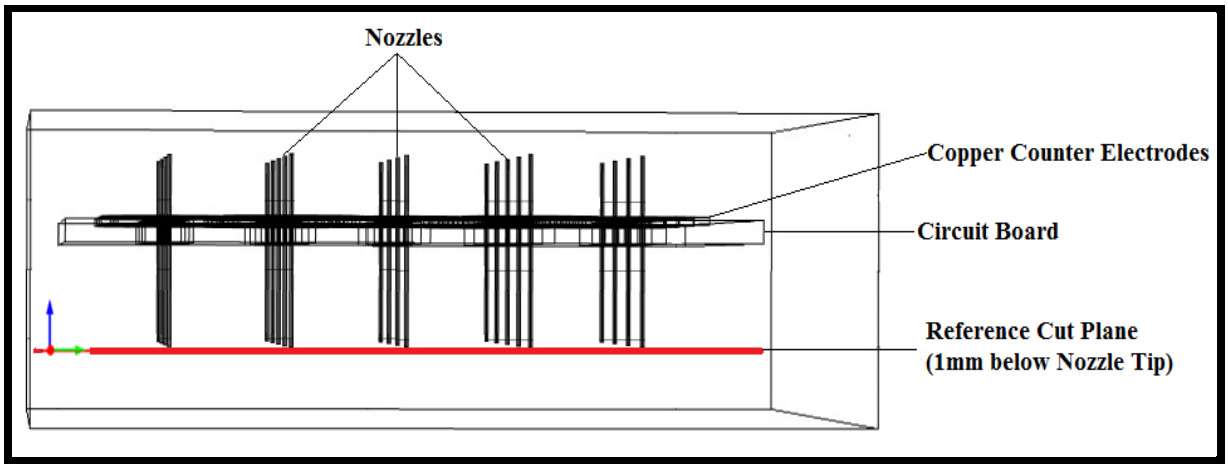

Figure 3.7: Snapshot of the 3D model geometry of the studied configuration

The counter electrode and nozzles were drawn to scale. It composed of 22 nozzles arranged in an alternating array of 4 nozzles in each array and 5 nozzles in the alternating array. The 4 nozzles array was replicated three times while the 5 nozzles array was replicated two times (Figure 3.7). All nozzles were equidistant to each other. 20 mm outer diameter, 15 mm inner diameter and 1 mm thick counter electrodes, positioned concentric to each nozzle, were placed 17 mm above the nozzle tip to model the electric field. The modeled nozzles had an outer diameter of 0.71 mm and were 25 mm long.

To get a good representation of the electric field, a reference cut plane at 1mm below the nozzles tip was chosen as done by Agostinho (2013).

3.8 Particle Tracing Modelling

In this section, modelling of the trajectories of particles produced by the 22 nozzle atomizer during the electrospray process was done. Modelling of these trajectories gave insights in the behaviour of the particles by illustrating the spray symmetry and particle dispersion at each nozzle. Particle tracing modelling may also be used to predict improvements to be made on the set-up which might lead to a better target deposition.

Comsol® Multiphysics version 4.4 was used to model the characteristics of the particle trajectories. It was done with the Charged Particle Tracing group of equations inside the 3D AC/DC module. The Charged Particle Tracing module allows for particles to be released inside the system and drew on the results of the Electrostatics module to determine the paths

of these particles. Therefore, particle tracing modelling is only done after the results of the electric field modelling have been received.

Comsol material library was used to define the physical properties of the modelled objects. The counter electrode material was defined as copper; the nozzle as stainless steel, insulation board as FR-4 (circuit board) and the surrounding material inside the box was set as air.

The boundaries conditions were defined as follows: The rings boundaries were defined with an electric potential of 6 kV. The nozzles boundaries were defined as grounded. The board boundaries were selected as dielectric shielding and the surroundings boundaries were selected as no charge. Droplet initial velocity was defined as 5 m/s as measured experimentally and which corresponds with the work done by Agostinho (2013).

3.9 Improvement of the Prototype

Once the prototype was fabricated, the operational window of the prototype was investigated. A better design was proposed at the end of the research as an improvement of the same based on the results obtained from performing experiments with the prototype and the limitations experienced.

3.10 Seawater Analyses

Seawater was sourced from the Indian Ocean along the Kenyan Coast at Mama Ngina Drive which lies at 4° 4' 44.04" S, 39° 40' 8.04" E. It was electrosprayed and two sets of the same sample, 30 millilitres each, were collected below the nozzles at the corresponding voltage and taken for analyses where 3 replicate samples were analysed. The analyses were carried out to assess any changes in trace elements' concentration with changes in the system voltage.

The 30 ml samples were collected as follows; one sample at the source (blank), another one prior to the electrospray process (0 kV) and seven samples after the process had occurred at different voltages in steps of one kilovolt. The samples were labelled and stored in pre-cleaned Polyethylene (PE) containers. A few drops of nitric acid were added to the samples to avoid metal adsorption.

The first set of the samples collected were shipped to the ICP-MS analytical laboratory of the Water Application Centre in the Netherlands in well labelled zip-lock polythene bags for analyses. Analyses of the samples as well as sample preparation were done according to procedures followed by Boye et al. (2012) and Beauchemin (2006).

The second set of the collected samples were placed in well labelled zip-lock polythene bags and shipped to the University of Nairobi, Institute of Nuclear Science and Technology, for TXRF analyses. Sample preparation and analyses of the samples were done following analytical procedure done by Chesori (2015) and Muohi et al., (2002).

4. RESULTS AND DISCUSSIONS

4.1 Introduction

Findings of the research study are presented in this chapter. Detailed analyses of results of the single effect chamber experiments were discussed. Results of the droplets attraction to tube experiments which were done to determine the required potential and the appropriate distance needed to attract the charged droplets were presented and discussed. These two studies were done to get acquainted with the electrospray technique and how to manipulate the droplets. Droplets size distribution, dispersion symmetry of the droplets and electric field for different applied voltages were presented and explained. Modelling results of both electric field and the subsequent particle trajectories were presented. Ultimately, the findings of the seawater samples analysed using TXRF and ICP-MS analysis techniques were presented and discussed.

4.2 Single Effect Chamber Experiment

Temperature measurements of the inlets and outlets for all three levels of the evaporation tube bundles were recorded for a period of 30 minutes for each of the applied voltage.

A correlation between the applied potential and the tube bundle temperature difference was presented (Figure 4.1).

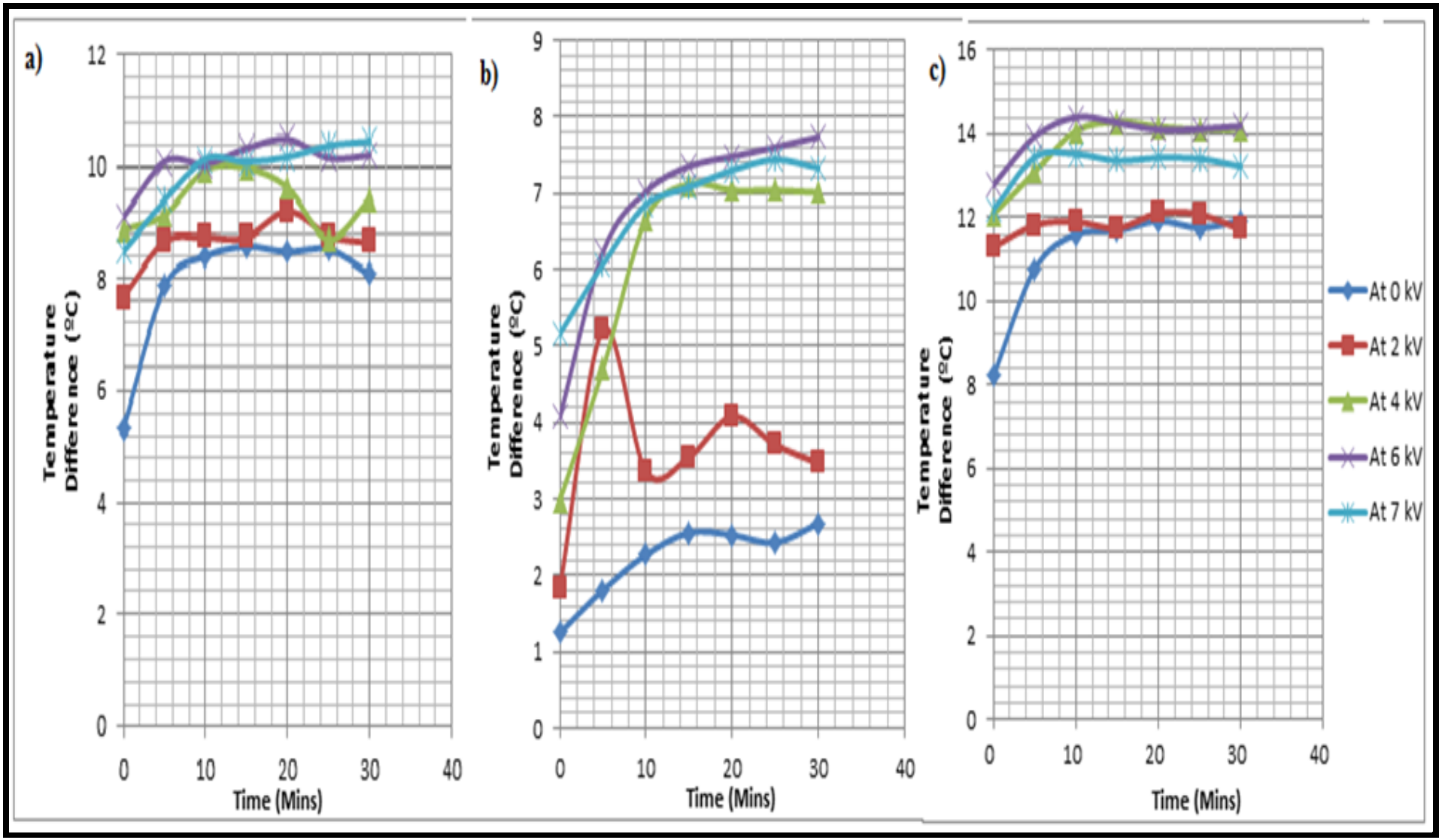

Figure 4.1 (a, b and c) : Temperature difference for top bundle (a) middle tube bundle (b) and bottom tube bundle (c).

Figure 4.1 shows an increase in voltage generally leads to an increase in the temperature difference for all of the tube bundles. This can be attributed to a better and wider dispersion of the electrosprayed droplets enlarging the wetting area on the tubes. The increased wetting area resulted in more droplets being evaporated on the tubes surfaces. The evaporated droplets carried the heat of vaporization with them causing a drop in the temperature of the liquid in the tubes. This caused the increased temperature difference o on the tubes' surface.

Nevertheless, the dispersed droplets did not cover the entire surface area of all the evaporation tube bundle. Therefore, a new multinozzle atomizer with more nozzles has to be designed to allow for proper coverage of the evaporation tube and eventually proper examination of the possible improvements in the tube bundle wetting ratio.

These experiments also showed that for a grounded tube, no attraction of the electrically charged droplets was observed for different tube bundles at different heights. This is possibly due to the fact that the field between the charged droplets and the grounded tube was not strong enough to attract the droplets to grounded tube. Further investigations to ascertain this phenomenon were done and were presented as well as discussed in section 4.3 - attraction of droplets to tube.

4.3 Droplets Attraction to Tube Experiments

The main objectives for performing droplets attraction to tube experiments was to determine the required potential and the appropriate minimum distance needed to attract the charged droplets to the evaporation tube without affecting the electrospray electric field.

For the uncharged tube and one nozzle experiments just like in the single effect chamber experiments, the droplets were not attracted to the tube surface when the tube was kept grounded. This fact was observed regardless of the tube to nozzle distances used.

For experiments with a charged tube and one nozzle, results have shown that the electrosprayed droplets could be attracted to the tube surface. However, attraction required different potential for different tube to nozzle distances (Figure 4.2). Attraction was obtained for negatively charged droplets (grounded nozzle and positively charged ring) with positively charged tubes and vice-versa. When the counter electrode was positively charged at 4 kV, the minimum voltages on the tube and tube to nozzle tip distance were tabulated (Table 4.1).

Figure 4.2: Attraction of Droplets to Tube

From table 4.1, it can be concluded that the lowest potential to provide droplet attraction to the charged tube was obtained at 20 cm. At that distance, attraction of the majority of the droplets to the tube surface was observed. Higher potential was required for shorter distances, e.g. 6, 8 and 10 cm, possibly due to the high acceleration of the droplets at that distance or the electric field interferences which could induce a different overall electric field configuration.

Table 4.1: Relation between minimum voltage on the tube and tube to nozzle tip distance.

Distance (cm)	Minimum voltage to attract droplets (kV)
6	12.39
8	10.31
10	10.75
20	8.28
30	9.9

At 2 cm and 4 cm, the voltage was increased until 13 kV but still the droplets were going underneath the pipe. At 13 kV, the droplets that went underneath the pipe were attracted back to the pipe on the other side. These droplets were seen along the whole tube of the other side.

4.4 Droplet Size Properties

The average droplet diameter measurements for all the nozzles were obtained by high speed imaging. An average measurement of 438 images recorded at 1000 frames per second of the

spray was done for each nozzle. The experiments were done for three different flow rates (360, 420 and 500 mL h^{-1} $nozzle^{-1}$) which were within the simple jet mode range and two different potentials (6 and 7 kV).

4.4.1 Mean Droplet Size

The mean droplet sizes were calculated with the use of Image J® software and Microsoft Excel® package to analyse the data obtained. Each nozzle was analysed individually then the mean of all the obtained droplets was calculated to illustrate the effect of increase of both the potential and the flow rate on the droplet size. The results of these investigations were tabled as table 4.2.

Table 4.2: Summarised values of Mean Droplets Diameters at different flow rates and different potentials

Flow rate per nozzle (mL/h)	Mean Diameter (mm)	
	6 kV	7 kV
360	1.24	1.21
420	1.17	1.15
500	0.97	0.95

In general, an increase in potential at constant flow rate and using the same type of nozzle caused a slight decrease in the mean droplet diameter (Table 4.2). This decrease was attributed to the increase in potential which caused decrease in the jet radius, (Hartman et al., 1999), which shortened the wavelength of the fastest growing perturbation and consequently the droplet size. Such behaviour is known and was reported in the study about the characteristics of the simple-jet mode by Agostinho et al. (2012).

The mean droplet size decreased with increase in flow rate at constant potential (Table 4.2). Increase in flow rate increases the number of droplets (Figure 4.3) therefore, when the mean of all the droplets was calculated, a decrease in the mean droplet diameter was observed.

To quantitatively describe the influence of the applied potential on the droplets size, Relative Standard Deviation (RSD) was used. Relative Standard Deviation (RSD) is defined as the ratio between the standard deviation and the mean diameter of the droplets. It was used to show the mono dispersity of the droplets if it was below ~0.2. Table 4.3 shows the relative standard deviation of droplets at different potentials and flow rates.

Table 4.3: Summarised mean droplets values of the relative standard deviation (RSD) of all of the measured nozzles at different potentials and at different flow rates.

Flow rate per nozzle (mL/h)	Relative Standard Deviation	
	6 kV	7 kV
360	0.30	0.29
420	0.34	0.32
500	0.37	0.36

Table 4.3 showed that the RSD was greater than 0.2. RSD greater than 0.3 signified that the droplets were poly dispersed. This was attributed to the different nozzles experiencing different electric field leading to difference in the droplet sizes. This concluded that the droplets were not of the same size. Further investigation to ascertain this phenomenon was done and was presented as well as discussed in the in section 4.6 - electric field modelling.

Nevertheless, increase in potential at constant flow rate led to reduction in RSD. This was observed in the three flow rates performed. This was an indication that application of potential improved the droplets size distribution.

4.4.2 Size Distribution

After investigating the mean droplet diameters at different voltages and flow rates, the droplet size distribution was measured. The experiments were done for three different flow rates (360, 420 and 500 mL h^{-1} $nozzle^{-1}$) which were within the simple jet mode range and two different potentials namely 6 and 7 kV (Figure 4.3).

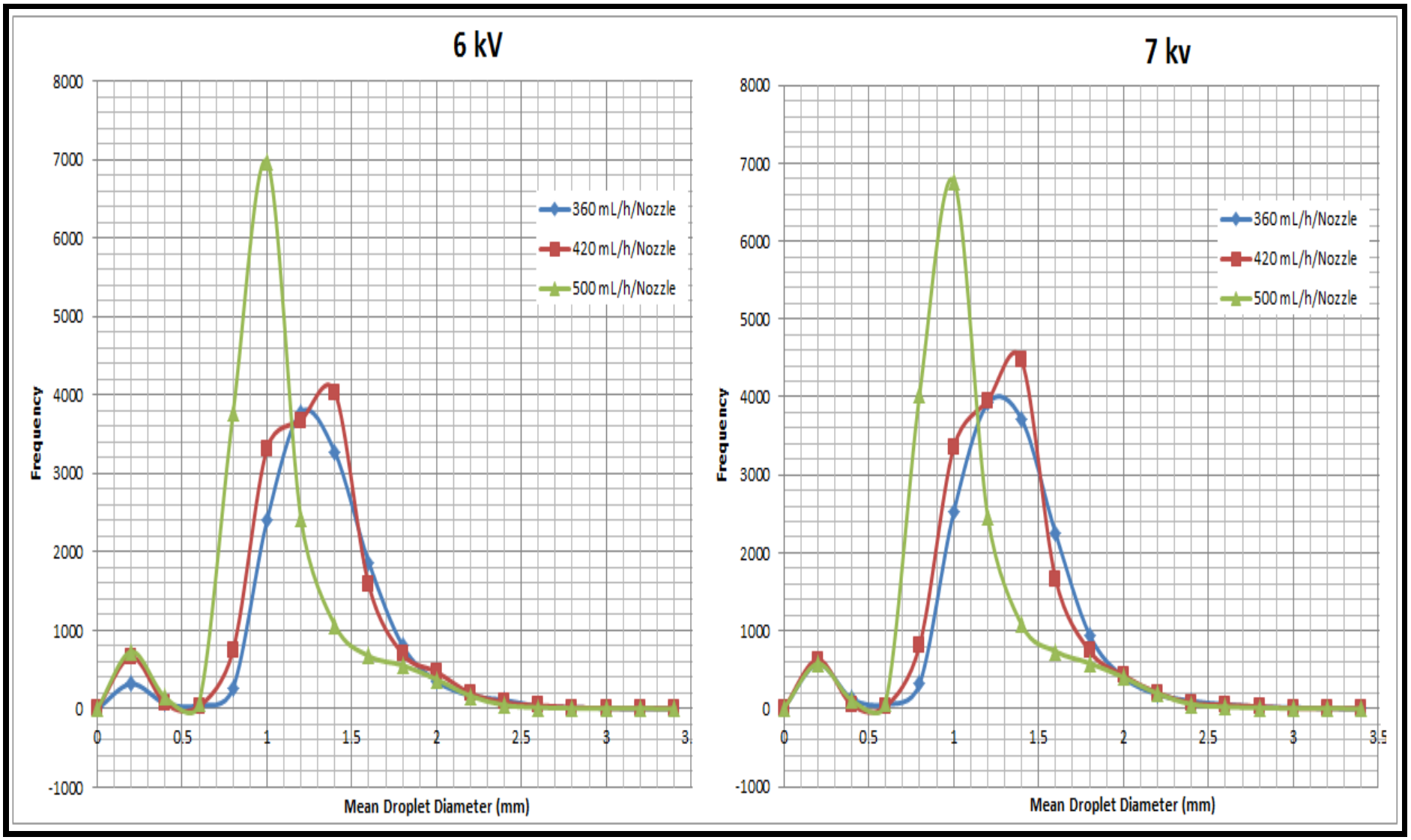

Figure 4.3 a) and b): Distribution of the droplet sizes from all the nozzles for a recorded time of 4 seconds for 6 (a) and 7 kV (b) respectively.

As observed in figure 4.3, the presence of a bimodal distribution in which two peaks namely the small peak (satellite droplets) and the major peak (primary droplets) was observed. The presence of satellite droplets, accounted for approximately 10% of all the droplets, compromises the mono dispersity of the droplets because they cause a second class of diameters (smaller than the primary droplets).

4.5 Droplets Dispersion

Dispersion of the produced droplets and spray symmetry was studied. Examinations of the spray for different flow rates and different electric potentials were done. The influence of the applied potential was observed since the dispersion of the droplets was enhanced as the applied potential increased (Figures 4.4, 4.5 and 4.6).

4.5.1 Bench Scale Experiments

Figures 4.4, 4.5 and 4.6 shows dispersion images of the multinozzle atomizer at flow rate of 360 mL h^{-1}, 420 mL h^{-1} and 500 mL h^{-1} under the influence of different potentials.

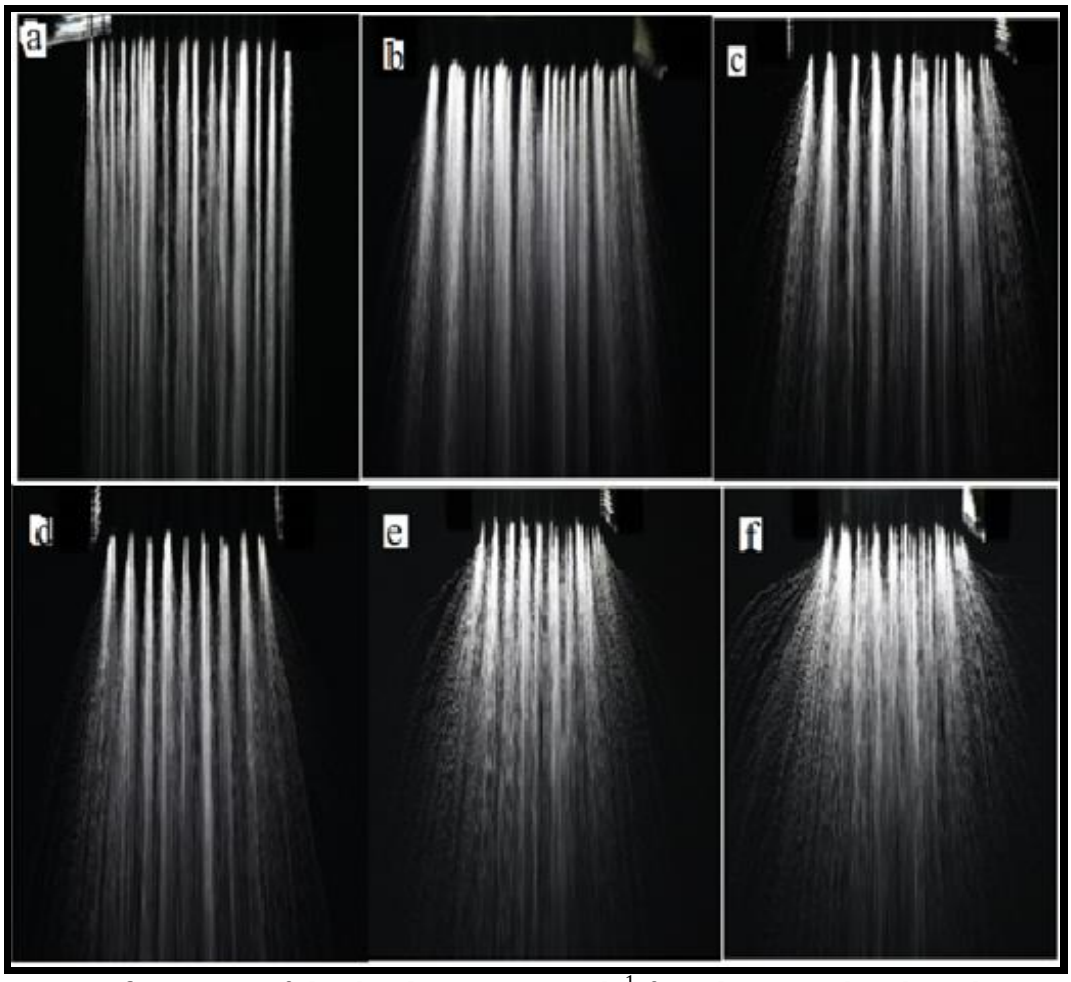

Figure 4.4 (a-f): Images of the droplets at 360 mL h^{-1} for 0 kV (a), 5 kV (b), 6 kV (c), 7 kV (d), 8 kV (e) and 9 kV (f).

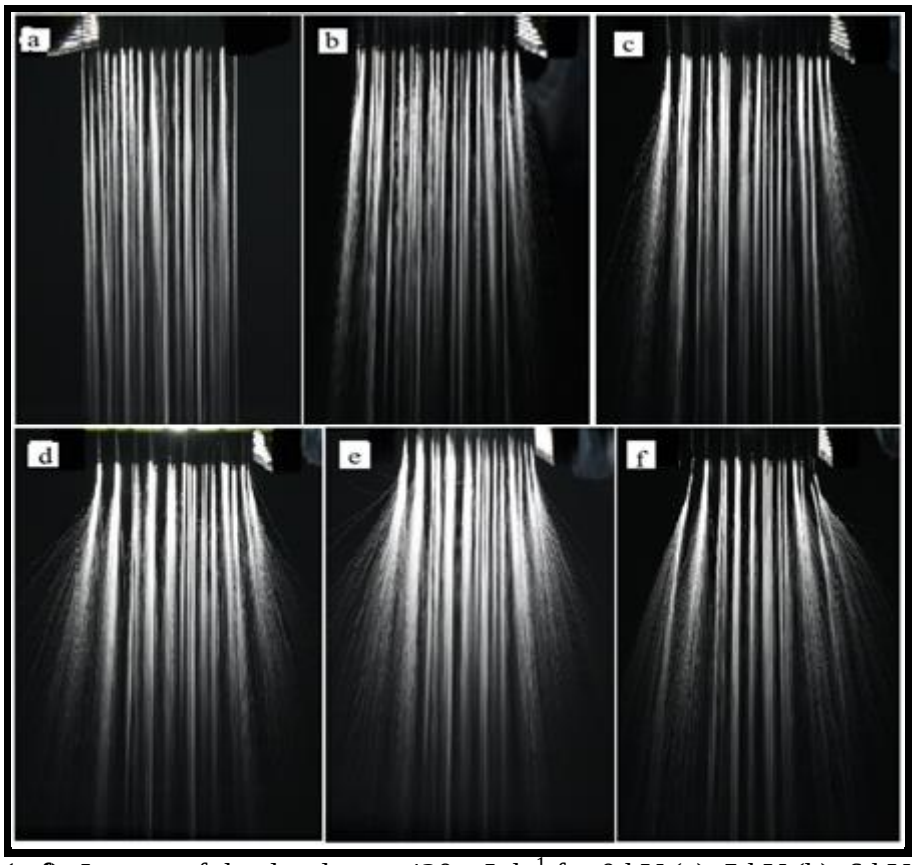

Figure 4.5 (a-f): Images of the droplets at 420 mL h^{-1} for 0 kV (a), 5 kV (b), 6 kV (c), 7 kV (d), 8 kV (e) and 9 kV (f).

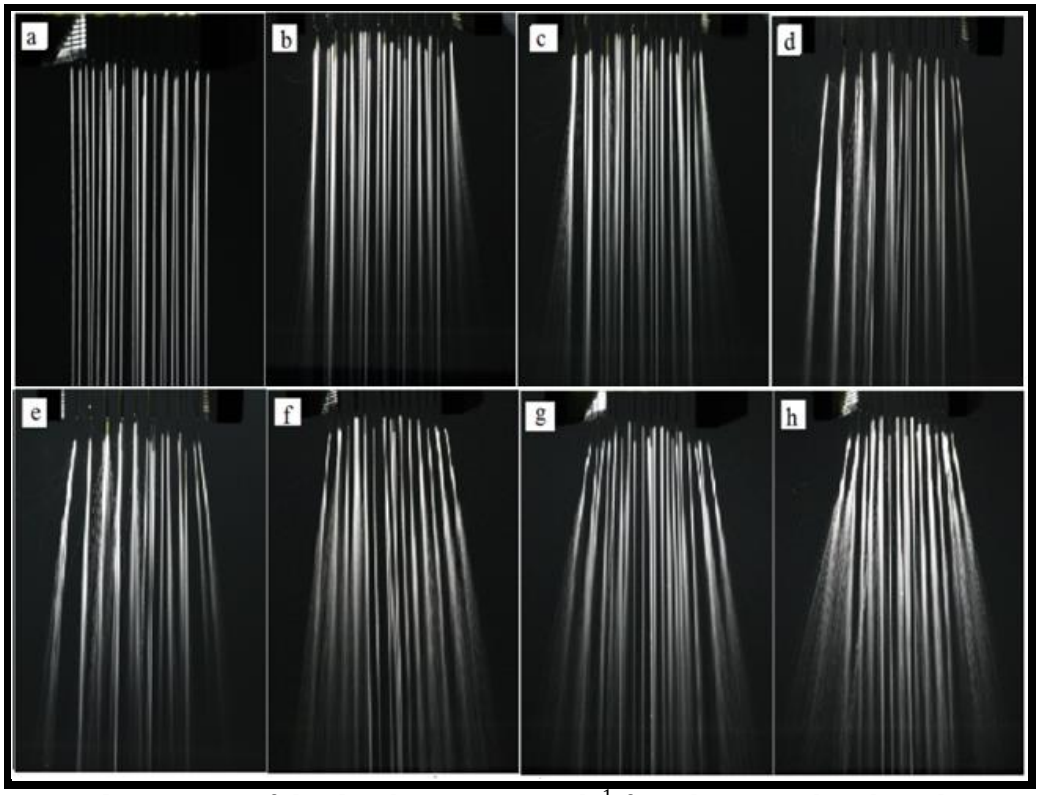

Figure 4.6 (a-h): Images of the droplets at 500 mL h^{-1} for 0 kV (a), 5 kV (b), 6 kV (c), 7 kV (d), 8 kV (e), 9 kV (f), 10 kV (g) and 11 kV (h).

It was observed that increase in applied voltage led to an increased dispersion of the droplets at a constant flow rate (Figures 4.4, 4.5 and 4.6). This result was attributed to the increased electric charge acquired by the droplets during atomization which caused a higher columbic repulsion of droplets thus the wider dispersion of droplets observed.

Dispersion of the droplets was seen to decrease with increase in flow rate (Figures 4.4, 4.5 and 4.6). This was due to the fact that higher flow rates have high droplets velocity. Thus, a higher potential was required to disperse the droplets further away so as to create a wider dispersion of droplets.

Since the device had a multinozzle configuration, edge effects were observed (Figures 4.4, 4.5 and 4.6). Edge effects are experienced when there is a deflection of the sprays at the periphery of the multinozzle atomizer (Arnanthigo et al, 2011). This phenomenon was evidenced by the wider dispersion of droplets of the outermost nozzles of the atomizer.

The inner nozzles were seen to have lesser dispersion of droplets when compared to the outer nozzles. This was because of their electric field was suppressed by the electric field of the surrounding nozzles thus their smaller dispersion of droplets.

4.5.2 Particle Tracing Modelling

Comsol® Multiphysics software was used to model the characteristics of the particle trajectories. The counter electrodes (rings) boundaries with an electric potential of 6 kV and the particle initial velocity defined as 5 m/s (Figure 4.7). 6 kV was chosen to imitate the conditions of the experiment and 5 m/s was defined after calculating the speed of the droplets in images and it was confirmed by Agostihno (2013) experiments on characteristics of the simple jet mode. The simulation cut plane was 50 cm below tips of the nozzles.

Displacement of the particles was observed for all of the nozzles (Figure 4.7). This result was due to the electric charge acquired by the particles during atomization which causes columbic repulsion amongst particles thus the displacement of particles from their original position.

Edge effects were observed (Figure 4.7). Edge effects are deflection of the sprays at the periphery of the multinozzle atomizer (Arnanthigo et al., 2011). This phenomenon was evidenced by the wider displacement of particles of the edge nozzles when compared with the rest of the nozzles.

The outermost nozzles have wider displacement of particles compared to the inner nozzles. This was because the particles from the inner nozzles are repulsed by the electric field of the surrounding nozzles hence their smaller displacement of particles.

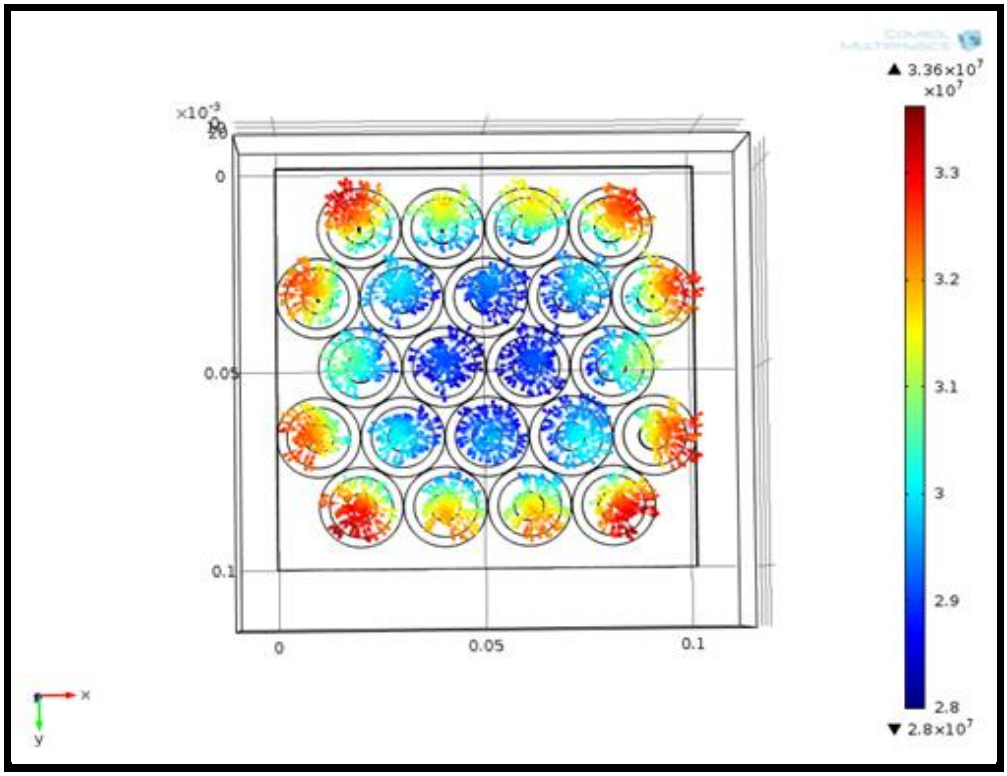

Figure 4.7: Particle Tracing Model. Applied potential of 6 kV (rings) with grounded nozzles with droplets initial velocity of 5 m/s. The simulation cut plane was 50 cm below tips of the nozzles. Colours represent the radial displacement of each particle from its initial position.

4.5.3 Comparison of the Experiments and the Model

Bench Scale Experiments showing the dispersion images of the multinozzle atomizer under different voltages were compared to the modelling results obtained by Comsol Multiphysics software and discussed in this section. Displacement of the particles in the model (Figure 4.7) and dispersion of the droplets in the experiments (Figure 4.4) were observed when voltage was applied. These showed that the experimental results matched with the modelling results.

Edge effects were also observed in both cases (Figure 4.4 and Figure 4.7) showing that the experimental results were similar to the model results.

The outermost nozzles had wider displacement of particles compared to the inner nozzles in the model (Figure 4.7) and a wider dispersion of droplets in the outermost nozzles than the inner nozzles for the case of the experiments (Figure 4.4). Thus, the model was in agreement with the experiment.

4.6 Electric Field Modelling

Figure 4.8 shows the resultant vector of the electric field at potential 6 kV and 1 mm below the nozzle as simulation cut plane.

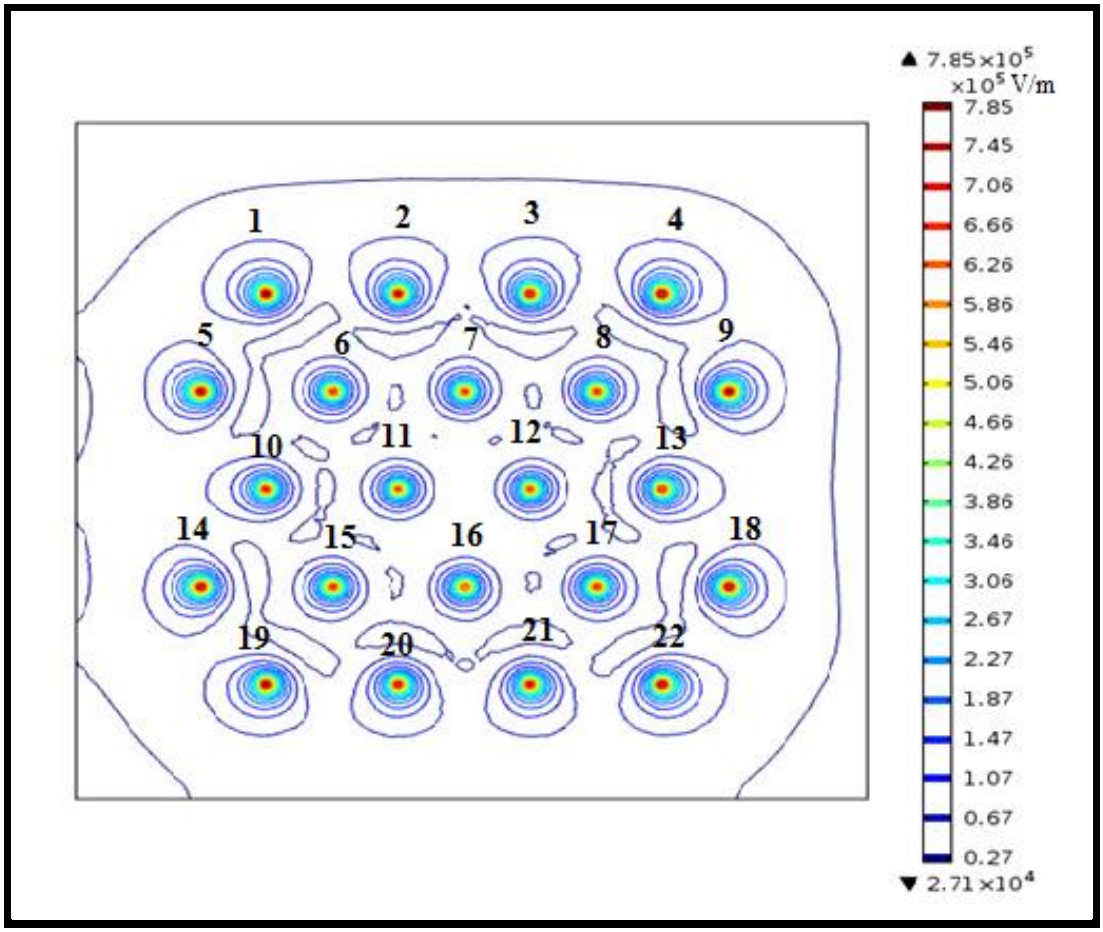

Figure 4.8: 2D Contour Plot of the Electric Field Strength (V/m) for the Multinozzle Atomizer. The circles represent equipotential lines. The plot show higher electric field intensity close to the nozzle tips.

As anticipated, the edge effect at the boundary of the atomizer that causes spray deflection was observed (Arnanthigo et al., 2011). This was evidenced by the irregular shape of the electric field of the outside nozzles (1, 2, 3, 4, 5, 9, 10, 13, 14, 18, 19, 20, 21 and 22). The

shape of their electric field was oval and were stretched outwards. This was because there was no electric field suppressing the outermost nozzles thus the edge effect.

Conversely, the remaining nozzles (6, 7, 8, 11, 12, 15, 16 and 17) had an almost regularly shaped electric field. This was because their electric fields were influenced by their surrounding nozzles' electric fields making them almost circular in shape.

Additionally, the middle array edge effects (10 and 13) have higher radial electric field magnitude than the other edge effects. This can be explained by the fact that the surrounding nozzles affecting the shape of the electric field were present in every direction except for the outside radial direction. Consequently, this led to increase in the electric field in the outside radial direction and eventually a wider displacement of particles in the outside radial direction.

6 kV was chosen for the simulation because this point is the optimum working condition of the device.

4.7 Improvement of the Prototype

Due to the limitations experienced by the first prototype, a second design was proposed. One major limitation as experienced with the first prototype was there was that less internal dispersion of droplets in inner nozzles, due to repulsion of individual droplets of closely spaced nozzles. This was proposed to be improved by spacing of the nozzles.

Since Agostinho (2013) and Brouwer (2011) 5-nozzle prototype was seen to have a wide dispersion at the middle nozzle, an outscale of that design in island form was proposed. 5-nozzle in star configuration with one at the middle of the star was selected as an island and four islands in a star configuration surrounded it. Each island had a diameter of 72 mm. The outer diameter of each copper counter electrode was 24 mm while the inner diameter was 19 mm. The surrounding islands were rotated 45° to create a compact design (Figure 4.9).

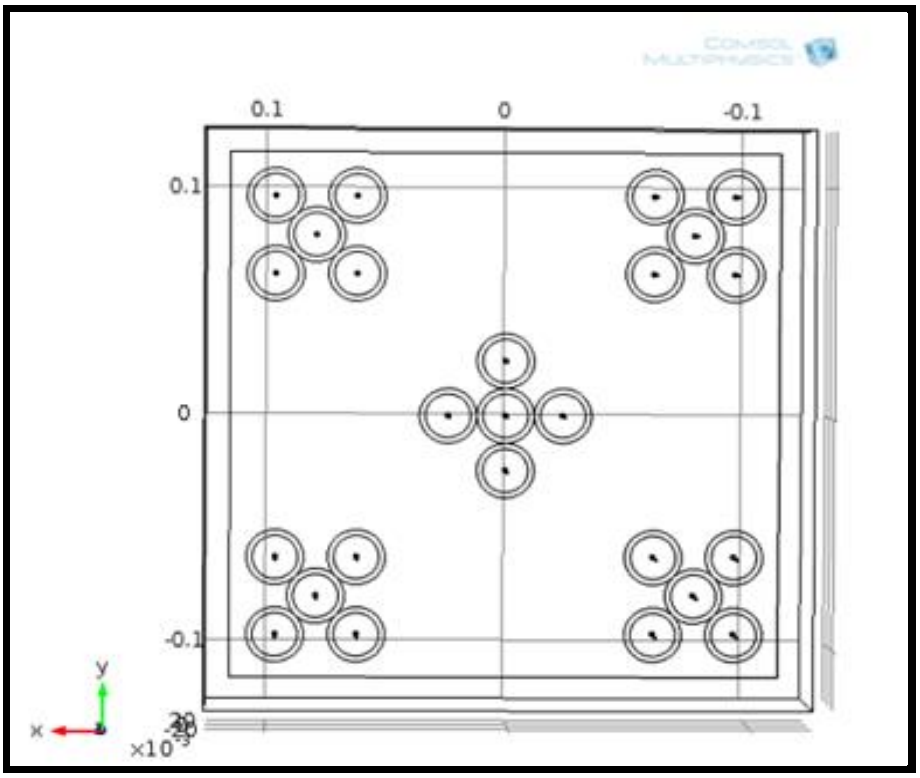

Figure 4.9: Proposed Multinozzle Configuration.

4.7.1 Electric Field Modelling

Comsol® Multiphysics software was used to model the characteristics of the electric field. The counter electrode material was defined as copper; the nozzle as stainless steel, insulation board as FR-4 (circuit board) and the surrounding material inside the box was set as air. The boundaries conditions were defined as follows: The ring boundaries were defined with an electric potential of 6 kV. The nozzles boundaries were defined as grounded. The board boundaries were selected as dielectric shielding and the surroundings boundaries were selected as no charge.

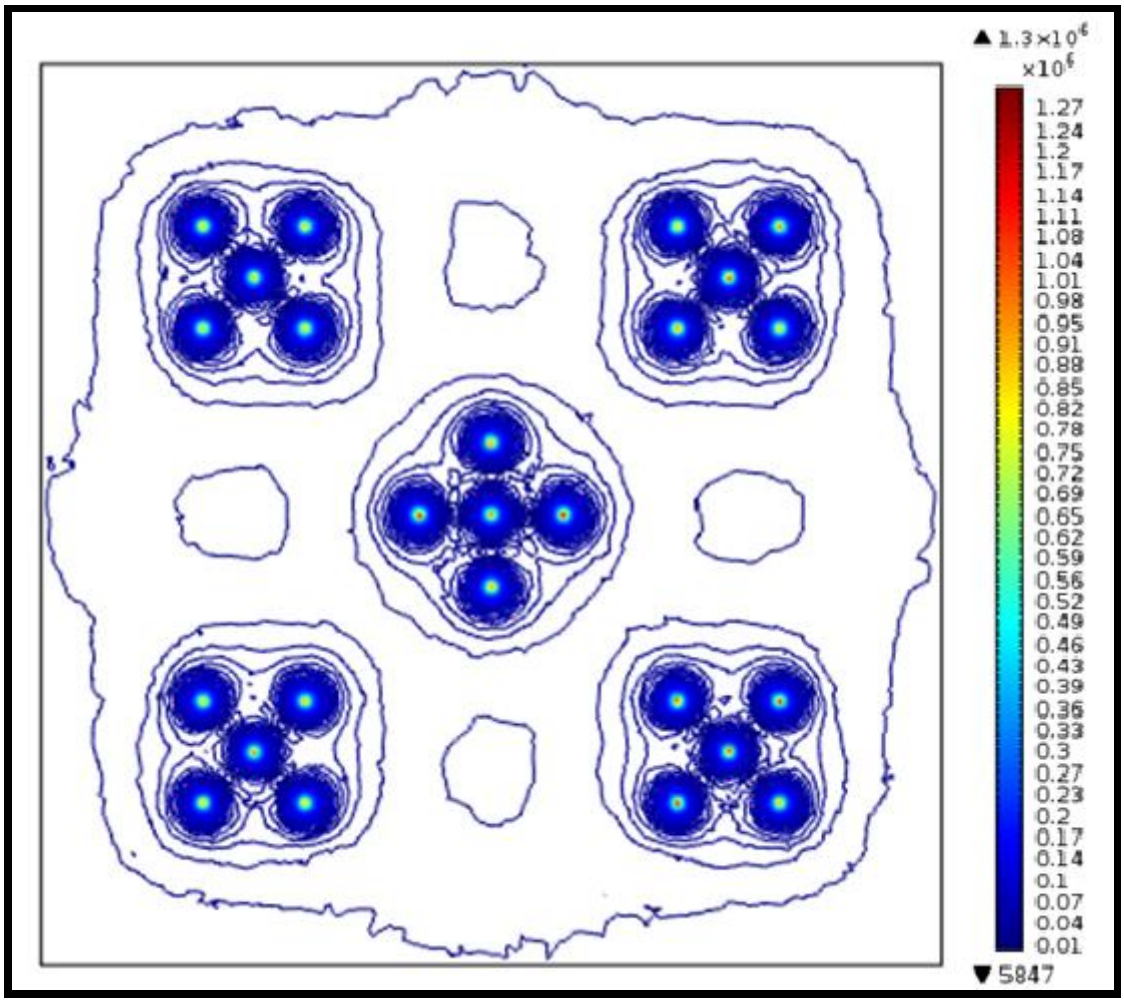

Figure 4.10: 2D Contour Plot of the Electric Field Strength (V/m) for the Proposed Multinozzle Configuration. The circles represent equipotential lines. The plot show higher electric field intensity close to the nozzle tips.

Figure 4.10 shows the resultant vector of the electric field at potential 6 kV and 1mm below the nozzle as simulation cut plane. The resultant electric field vector is the axial and radial electric field component in each point. Unlike the first prototype, all the nozzles in this configuration were seen to experience the same electric field.

Additionally, the islands of nozzles were experiencing similar electric field. This is an indication that all the nozzles in this configuration were seen to experience the same electric field.

4.7.2 Particle Tracing Modelling

Comsol® Multiphysics software was used to model the characteristics of the particle trajectories. The counter electrodes (rings) boundaries with an electric potential of 6 kV and the particle initial velocity was chosen to be as 5 m/s (Figure 4.11) after calculating the speed of the droplets using images in Image J®. 6 kV was chosen to imitate the conditions of the experiment.

Displacement of the particles was observed, 50 cm below the tip of the nozzles, for all of the nozzles (Figure 4.11). This result was due to the electric charge acquired by the particles during atomization which causes columbic repulsion of particles thus the displacement of particles from their original trajectory.

It was also observed that there was uniform dispersion of droplets in all of the nozzles (Figure 4.11 (a)). This was because droplets of different nozzles did not interfere with each other as there was enough space for the droplets to disperse. Therefore, spacing of the nozzles improved the dispersion of the droplets and was the solution of the limitation experienced by the first prototype.

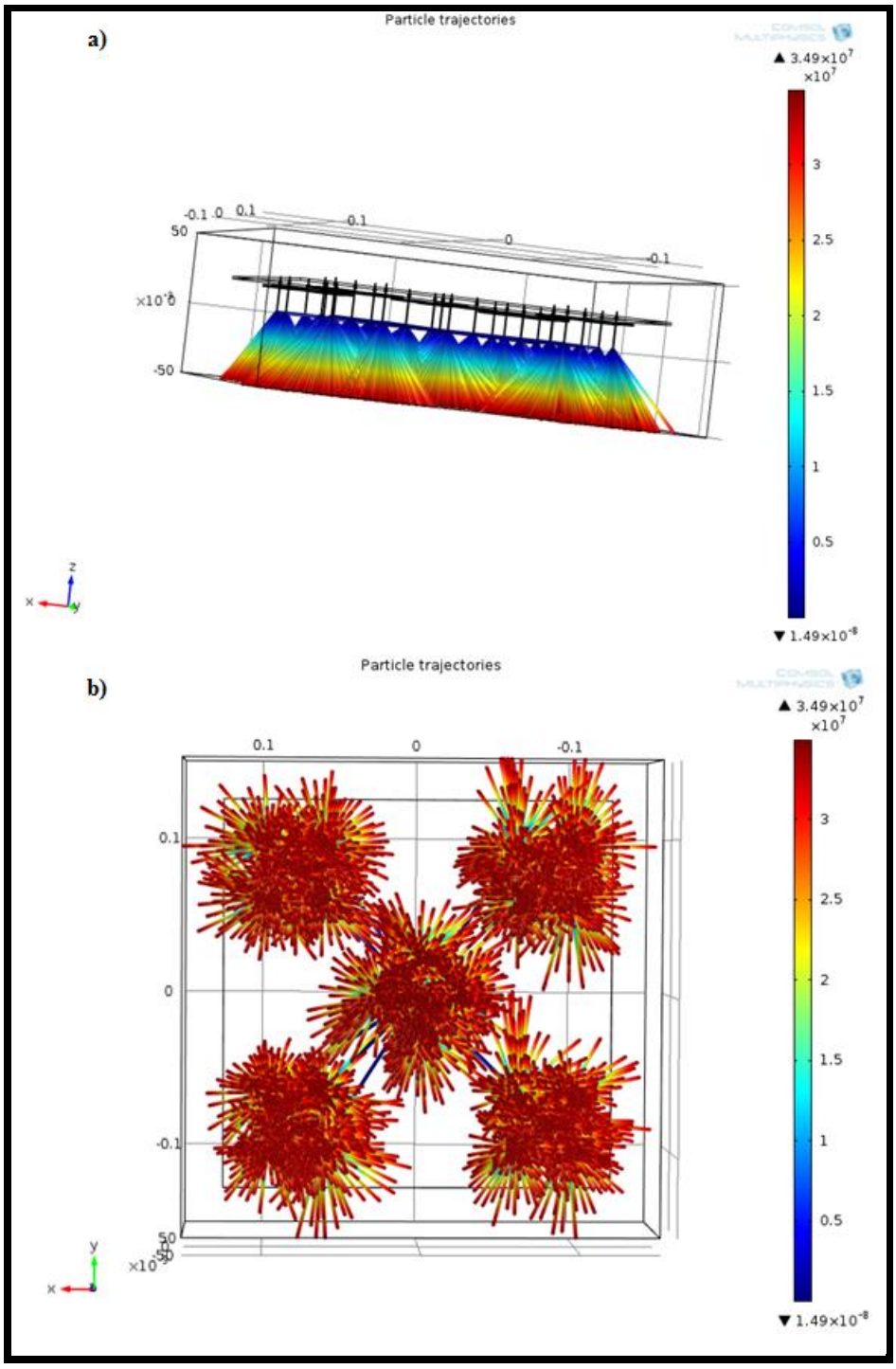

Figure 4.11 (a) and (b): Particle Tracing Model Side view (a) and Bottom view (b). Applied potential of 6 kV (rings) with grounded nozzles with droplets initial velocity of 5 m/s. Colours represent the radial displacement of each particle from its initial position.

4.8 Seawater Analyses

This section presents the findings of the analysed seawater samples. The results of the corresponding elemental concentration were given in mass per unit volume of the collected liquid.

The collected samples were analysed using Inductively Coupled Plasma Mass Spectrometry (ICP-MS) (Table 4.4) and Total X-Ray Fluorescence (Table 4.5) methods.

Table 4.4: Elemental concentrations of seawater samples analysed by ICP-MS

Voltage	Elemental Concentration (mg l^{-1})			
(kV)	Cl	K	Ca	Cu
Blank	21900	321	165	0.12
0	21300	370	238	0.21
1	22500	295	345	0.26
2	21800	321	334	0.30
3	19500	318	350	0.33
4	18000	309	405	0.34
5	19000	382	408	0.36
6	17200	302	412	0.37
7	18000	315	433	0.40

Table 4.5: Elemental concentrations of seawater samples analysed by TXRF

Voltage	Elemental Concentration (mg l^{-1})			
(kV)	Cl	K	Ca	Cu
Blank	12146	207	395	0.11
0	7282	137	311	0.09
1	10317	147	332	0.08
2	7916	168	336	0.10
3	7764	245	232	0.10
4	9537	192	343	0.12
5	7725	216	332	0.14
6	7141	142	266	0.10
7	9180	205	389	0.12

It was observed that all the evaluated elemental concentrations of Cl, K, Ca and Cu remained similar with increasing voltage in both analytical methods (Table 4.4 and 4.5). However, the two methods gave results which were a factor of less than three between ICP-MS and TXRF (Table 4.6).

Table 4.6: The ratio of elemental concentration values obtained from ICP-MS to TXRF

Voltage	ICP-MS to TXRF Concentration Ratio			
(kV)	Cl	K	Ca	Cu
Blank	1.8	1.6	0.4	1.0
0	2.9	2.7	0.8	2.3
1	2.2	2.0	1.0	3.3
2	2.8	1.9	1.0	3.0
3	2.5	1.3	1.5	3.3
4	1.9	1.6	1.2	2.8
5	2.5	1.8	1.2	2.6
6	2.4	2.1	1.5	3.7
7	2.0	1.5	1.1	3.3

The observed elemental concentration values from the two analytical techniques were observed to undergo negligible change with varying voltage implying minimal evaporation. Under droplets evaporation, increased concentration of trace elements in sea water would be expected. However, further investigation is needed to establish the reason why the concentration in blank and at 0 kV exhibited some difference.

5. CONCLUSION AND RECOMMENDATIONS

5.1 Conclusion

The design and characterisation of an electrohydrodynamic multinozzle atomizer for thermal desalination processes was done. Therefore, the main objective was achieved.

Additionally, outscaling of Agostinho's (2013) and Brouwer's (2011) work was done as the packing density of the prototype was found to be $2.2*10^3$ nozzles m^{-2} compared to $1.2*10^3$ nozzles m^{-2} packing density used by Agostinho (2013) and Brouwer (2011). This was approximately double their packing density.

Electrospraying using this prototype in the simple jet mode of 0.5 L $nozzle^{-1}$ was found to have a higher liquid output of 11 L h^{-1} compared to 2.2 L h^{-1} used by Agostinho (2013) and Brouwer (2011). It has five times the liquid output.

Computational models to check the process parameters were simulated. It was observed that the outermost nozzles have wider displacement of particles compared to the inner nozzles. This was because the particles from the inner nozzles are repulsed by the electric field of the surrounding nozzles thus their smaller displacement of particles.

Bench scale results concluded that the application of an electric field caused the droplets of the outermost nozzles to have wider displacement of particles compared to the inner nozzles and there was reduction in droplet diameter with increase in voltage.

The particle trajectories and electric field modelling matched the bench scale results.

Application of high voltage during the electrospray process caused no changes in the elemental concentration of seawater implying there was no evaporation of water through the system. However, more investigation is necessary.

Due to the limitations experienced by the first prototype, a second design was proposed. It showed increased dispersion of inner nozzles. This was increased by using four islands of 5-nozzles each in star configuration with one at the middle of the star and the surrounding islands rotated 45° to create a compact design.

5.2 Recommendations

- Further research needs to be done to confirm the optimal distance between the nozzles that will not affect the integrity of the multinozzle atomizer when coupled with an evaporator.
- There is need to conduct research to confirm the optimal island to island configuration that can be used to yield the highest possible density that will not affect the integrity of the multinozzle atomizer when coupled with an evaporator.
- The researcher further proposes research studies to be conducted to determine the best droplet size and shape to be used on the evaporator.
- The next phase of this research is the design and development of the evaporator system for this atomizer.
- Solar energy powering for the complete device may be considered as an alternative energy source for this system.

REFERENCES

Agostinho, L. L. F. (2013). *Electrohydrodynamic Atomization in the Simple-Jet Mode: Out-scaling and Application.* (PhD Dissertation), Delft University of Technology, Delft, The Netherlands.

Agostinho, L. L. F., Tamminga, G., Yurteri, C. U., Brouwer, S. P., Fuchs, E. C., and Marijnissen, J. C. M. (2013a). Morphology of water electrosprays in the simple-jet mode. *Physical Review E, 86*(6).

Agostinho, L. L. F., Yurteri, C. U., Fuchs, E. C., and Marijnissen, J. C. M. (2012). Monodisperse water microdroplets generated by electrohydrodynamic atomization in the simple-jet mode. *Applied Physics Letters, 100*(24).

Agostinho, L. L. F., Yurteri, C. U., Wartena, J., Brouwer, S. P., Fuchs, E. C., and Marijnissen, J. C. M. (2013b). Insulated multinozzle system for electrohydrodynamic atomization in the simple-jet mode. *Applied Physics Letters, 102*(19).

Arnanthigo, Y., Yurteri, C.U., Biskos, G., Marijnissen, J.C.M., and Schmidt-Ott, A. (2011). Out-scaling electrohydrodynamic atomization systems for the production of well-defined droplets. *Powder Technology, 214* 382–387.

Ashgriz, N., and Yarin, A.L. (Eds.). (2011). *Capillary Instability of Free Liquid Jets*. New York: Springer.

Beauchemin, D. (2006). Inductively coupled plasma mass spectrometry. *Analytical Chemistry, 78,* 4111- 4136.

Bocanegra, R., Galán, D., Márquez, M., Loscertales, I.G., and Barrero, A. (2005). Multiple electrosprays emitted from an array of holes. *Aerosol Science, 36*, 1387–1399.

Boye, M., Wake, B. D., Garcia, P. L, Bown, J., Baker, A. R., and Achterberg, E. P. (2012). Distributions of dissolved trace metals (Cd, Cu, Mn, Pb, Ag) in the Southeastern Atlantic and the Southern Ocean. *Biogeosciences*, 9, 3231–3246.

Brouwer, S. P. (2011). *Design and Characterisation of a Single-effect Electrohydrodynamic Desalinator.* (Masters Degree), Delft University of Technology, Leeuwarden, The Netherlands.

Chesori, R. C. (2015). *Determination of elemental concentrations in edible seaweeds, sea sediments and seawater samples from the Kenyan Coast using X-ray Fluorescence techniques.* (Masters Degree), University of Nairobi, Nairobi, Kenya.

Clanet, C., and Lasheras, J. C. (1999). Transition from dripping to jetting. *Fluid Mechanics, 383*, 307-326.

Cloupeau, M., & Prunet-Foch, B. (1994). Electrohydrodynamic spraying functioning modes: A critical review. *Journal of Aerosol Science*, 25(6), 1021-1036.

Degremont. (2014). Reverse Osmosis. Retrieved 31st August, 2014 from http://www.degremont.com/en/know-how/municipal-water-treatment/desalination/reverse-osmosis/processes/

Deng, W., Waits, C. M., Morgan, B., and Gomez, A. (2009). Compact multiplexing of monodisperse electrosprays. *Aerosol Science, 40,* 907-918.

El-Dessouky, H. T., and Ettouney, H. M. (2002). *Fundamentals of Salt Water Desalination* (1st Edition). Amsterdam: Elsevier Science B.V.

Ettouney, H., and Wilf, M. (Eds.). (2009). *Commercial Desalination Technologies* (Vol. 01). Palermo: Springer.

GOK (2007). *Kenya Vision 2030*. Nairobi, Kenya. : Government Publishers.

Geerse, K. B. (2003). *Application of Electrospray: From people to plants*. (PhD Dissertation), Delft University of Technology, Delft, The Netherlands.

Grace, J. M., and Marijnissen, J. C. M. (1994). A Review of Liquid Atomization by Electrical Means. *Aerosol Science, 25*(6), 1005-1019.

Hartman, R. P. A., Brunner, D. J., Camelot, D. M. A. Marijnissen, J. C. M., and Scarlett, B. (1999). Electrohydrodynamic atomization in the cone-jet Mode physical modelling of the liquid cone and jet. *Journal of Aerosol Science***,** 30 (7), 823 – 849.

Hartman, R. P. A. (1998). *Electrohydrodynamic Atomization in the Cone-Jet Mode: From Physical Modelling to Powder Production.* (PhD Dissertation), Delft University of Technology, Delft, The Netherlands.

Jaworek, A. , & A., Krupa. (1999). Classification of the modes of EHD Spraying. *Aerosol Science*, 30(7), 873 - 893.

IAEA (2003). *Development and use of reference materials and quality control methods*. Vienna: International Atomic Energy Agency.

Jingwei, H. C., Cheng, H., Wang, D., Gao X. and Gao, C. (2010). Experimental investigation of low temperature distillation coupled with spray evaporation. *Desalination, 258*, 5–11.

KIHBS (2005/2006). *Kenya Integrated Household Budget Survey*. Nairobi: Government Printer. Retrieved from http://statistics.knbs.or.ke/nada/index.php/catalog/8.

Klockenkämper (1997). *Total-Reflection X-Ray Fluorescence Analysis*. New Delhi: John Wiley & Sons.

MDG (2014). Ensuring Environmental Sustainability. Retrieved 31st August, 2014, from http://www.un.org/millenniumgoals/environ.shtml

Micale, Giorgio, Cipollina, Andrea, and Rizzuti, Lucio (Eds.). (2009). *Seawater Desalination for Freshwater Production* (Vol. 01). Palermo: Springer.

Muohi, A. W., Onyari, J. M., Omondi, J. G. and Mavuti, K. M. (2002). Heavy metals in sediments from Makupa Creek and Port-Reitz Creek systems of Kenyan Coast. *Environmental International, 28*, 639-647.

Processes, Separation. (2014a). Multi-Effect Distillation. Retrieved 31st August, 2014 from http://www.separationprocesses.com/Distillation/Multieffect/

Processes, Separation. (2014b). Multi-Stage Flash Distillation. Retrieved 31st August, 2014 from http://www.separationprocesses.com/Distillation/Flash/

SDG (2015). Ensure access to water and sanitation for all. Retrieved 30th September, 2015, from http://www.un.org/sustainabledevelopment/water-and-sanitation/

Skoog, D. A., Holler, F. J., and Crouch, S. R. (2007). *Principles of Instrumental Analysis* (Sixth ed.). Canada: Thomson Brooks/Cole.

Van-Hoeve, W., Gekle, S., Snoeijer, J. H., Versluis, M., Brenner, M. P., and Lohse, D. (2010). Breakup of diminutive Rayleigh jets. *Physics of Fluids, 22*(12).

Voica, C., Dehelean, A., Iordache, A., and Geana, I. (2012). Method validation for determination of metals in soils by ICP-MS. *Romanian Reports in Physics*, *64*, (1), 221–231.

WHO (2011). *Safe Drinking-water from Desalination*. Geneva: World Health Organization.

WHO (2012). *UN-Water Global Analysis and Assessment of Sanitation and Drinking Water Report: The challenge of extending and sustaining services.* Geneva: United Nation Water.

WWF (2007). *Desalination: Option or distraction for a thirsty world?* , Retrieved 31st August, 2014 from http://www.melaleucamedia.com/

Wang, J., Balazs, M., Pianetta, P., Baur, K. and Brennan, S. (2000). *Analytical Techniques for Trace Elemental Analyses on Wafer Surfaces for Monitoring and Controlling Contamination.* Proceedings of Semiconductor Pure Water and Chemicals Conference, Santa Clara, CA.

Wang, L. K., Chen, J. P., Hung, Y., and Shammas, N. K. (2011). *Membrane and Desalination Technologies: Handbook of Environmental Engineering.* New York: Springer.

Yurteri, C. U., Hartman, R.P.A., and Marijnissen, J.C.M. (2010). Producing Pharmaceutical Particles via Electrospraying with an Emphasis on Nano and Nano Structured Particles - A Review. *KONA Powder and Particle, 28*, 91-115.

APPENDIX

Detailed Engineering Drawings

In this section, assembly and detail drawings of different components of the electrohydrodynamic multinozzle atomizer were presented.

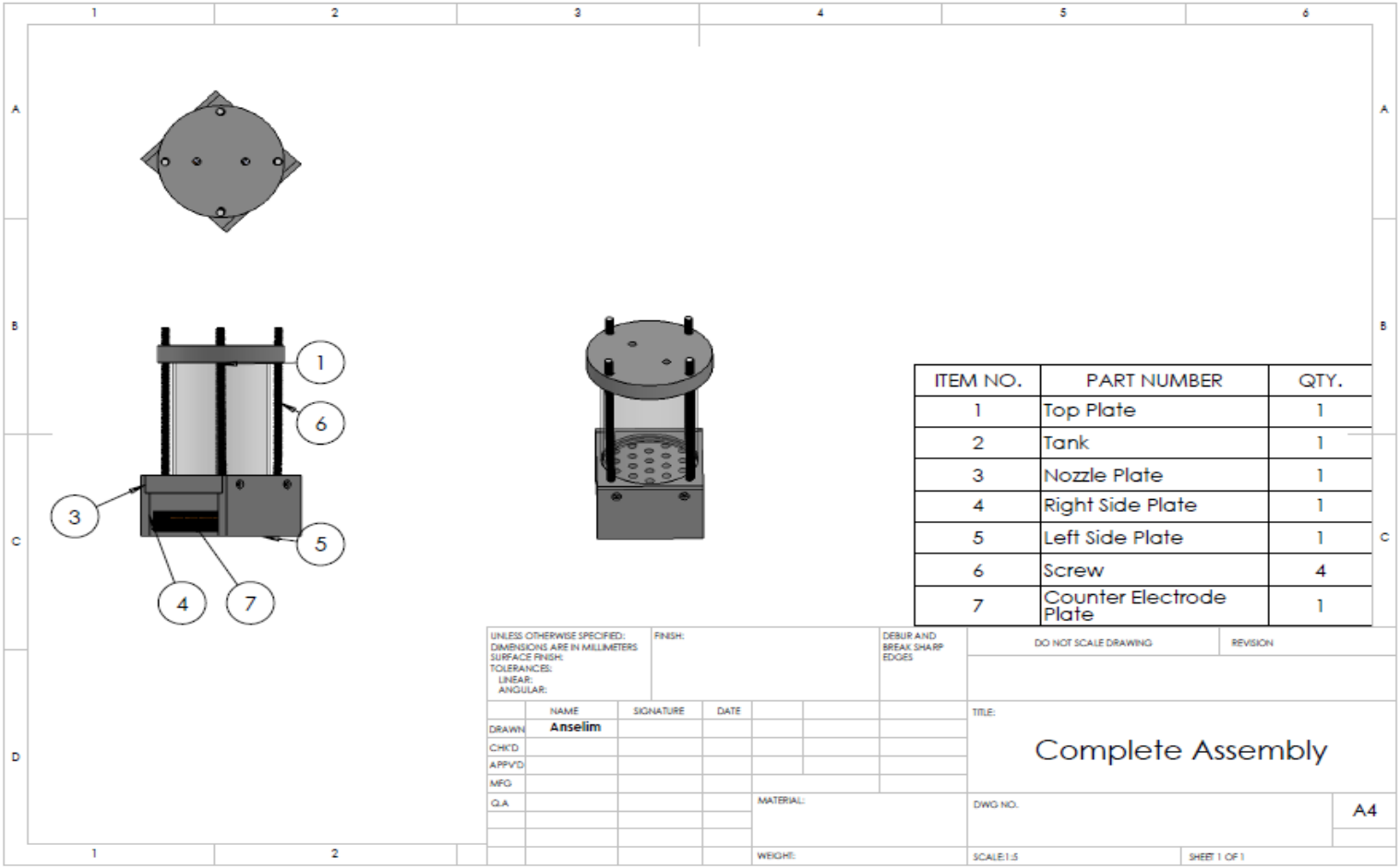

ITEM NO.	PART NUMBER	QTY.
1	Top Plate	1
2	Tank	1
3	Nozzle Plate	1
4	Right Side Plate	1
5	Left Side Plate	1
6	Screw	4
7	Counter Electrode Plate	1

UNLESS OTHERWISE SPECIFIED:
DIMENSIONS ARE IN MILLIMETERS
SURFACE FINISH:
TOLERANCES:
LINEAR:
ANGULAR:

FINISH:

DEBUR AND BREAK SHARP EDGES

DO NOT SCALE DRAWING | REVISION

	NAME	SIGNATURE	DATE
DRAWN	Anselim		
CHK'D			
APPV'D			
MFG			
Q.A			

MATERIAL:

WEIGHT:

TITLE: Complete Assembly

DWG NO. A4

SCALE:1:5 | SHEET 1 OF 1

Figure 7.1: Complete Assembly

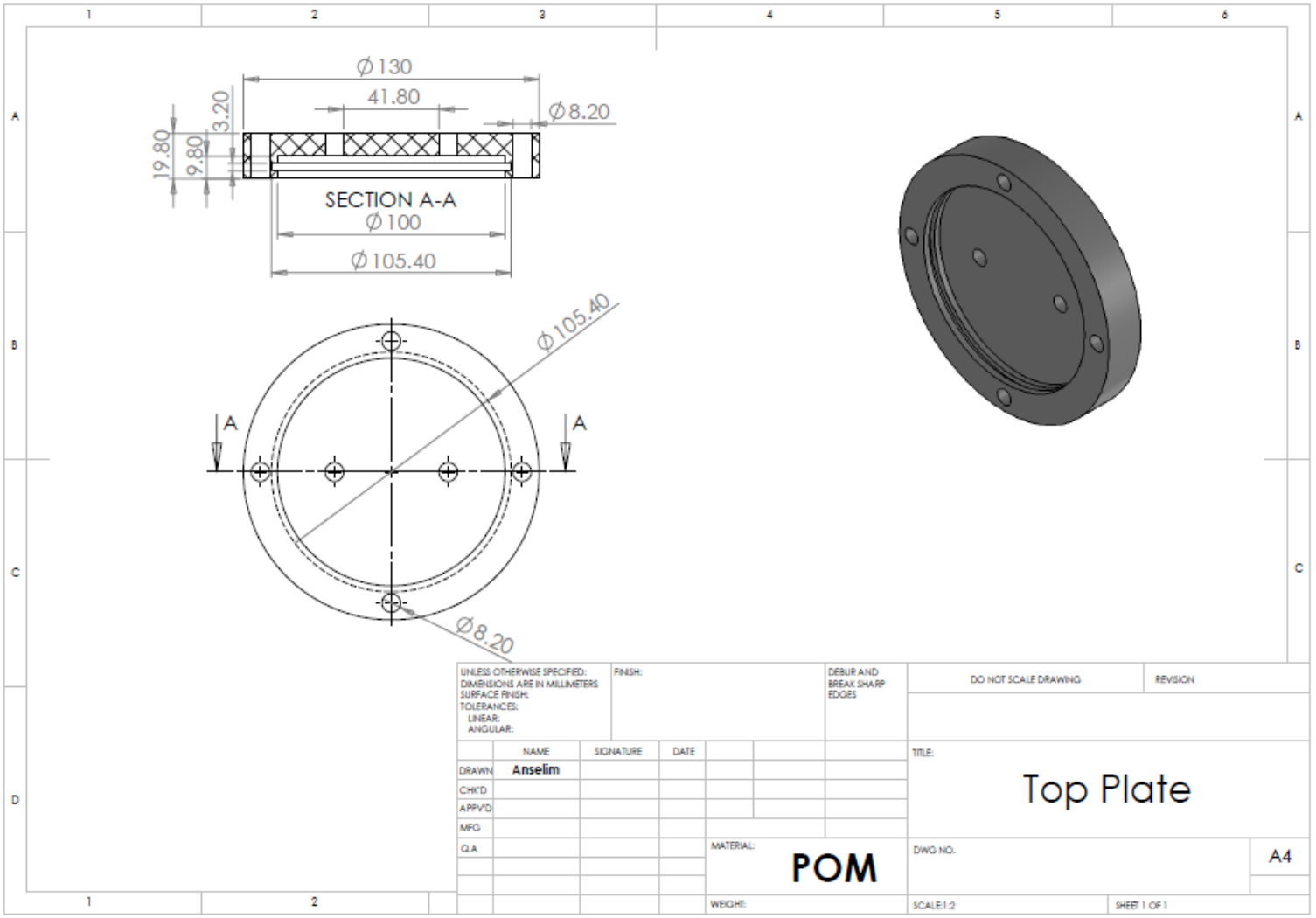

Figure 7.2: Top Plate

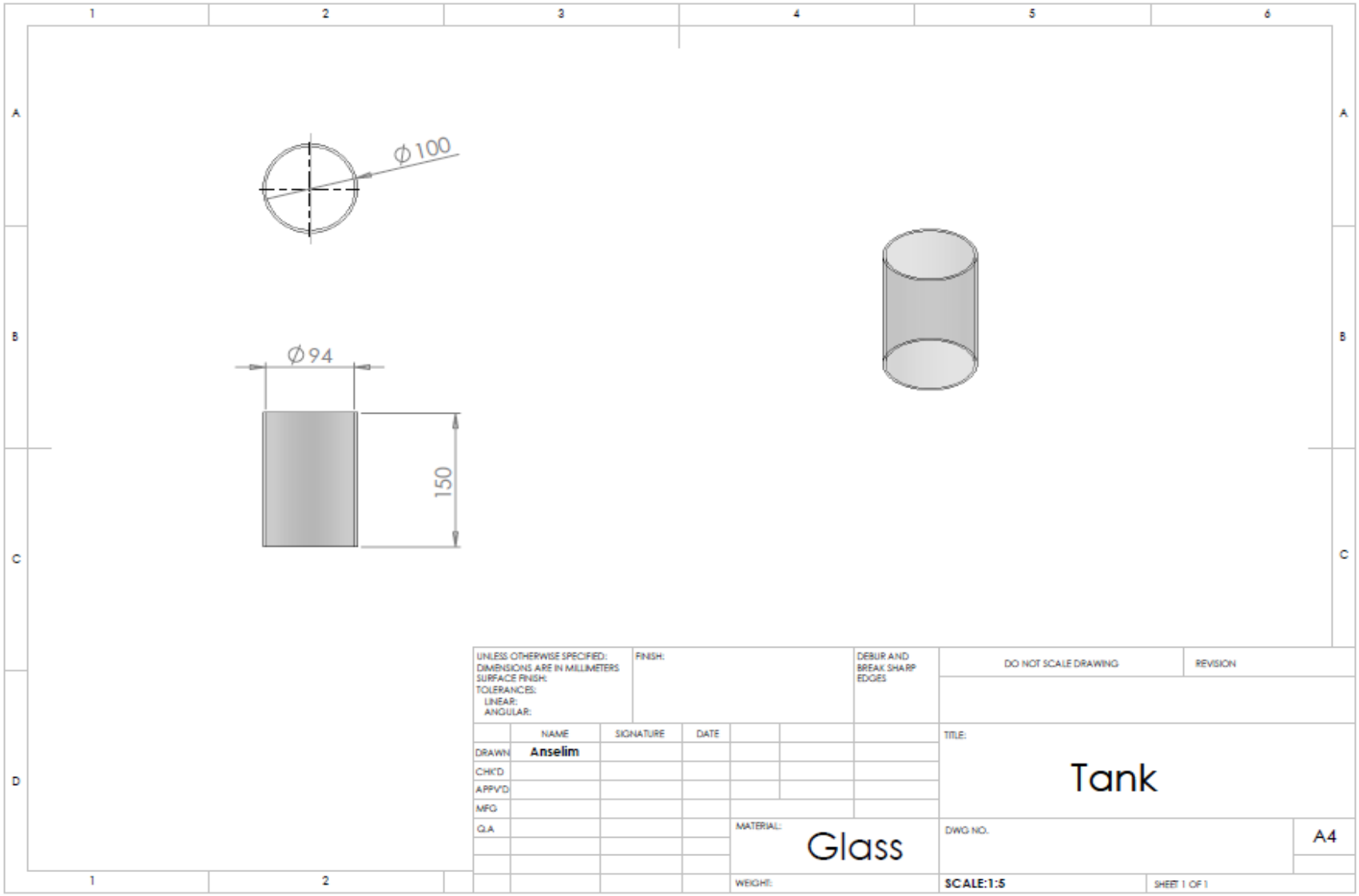

Figure 7.3: Tank

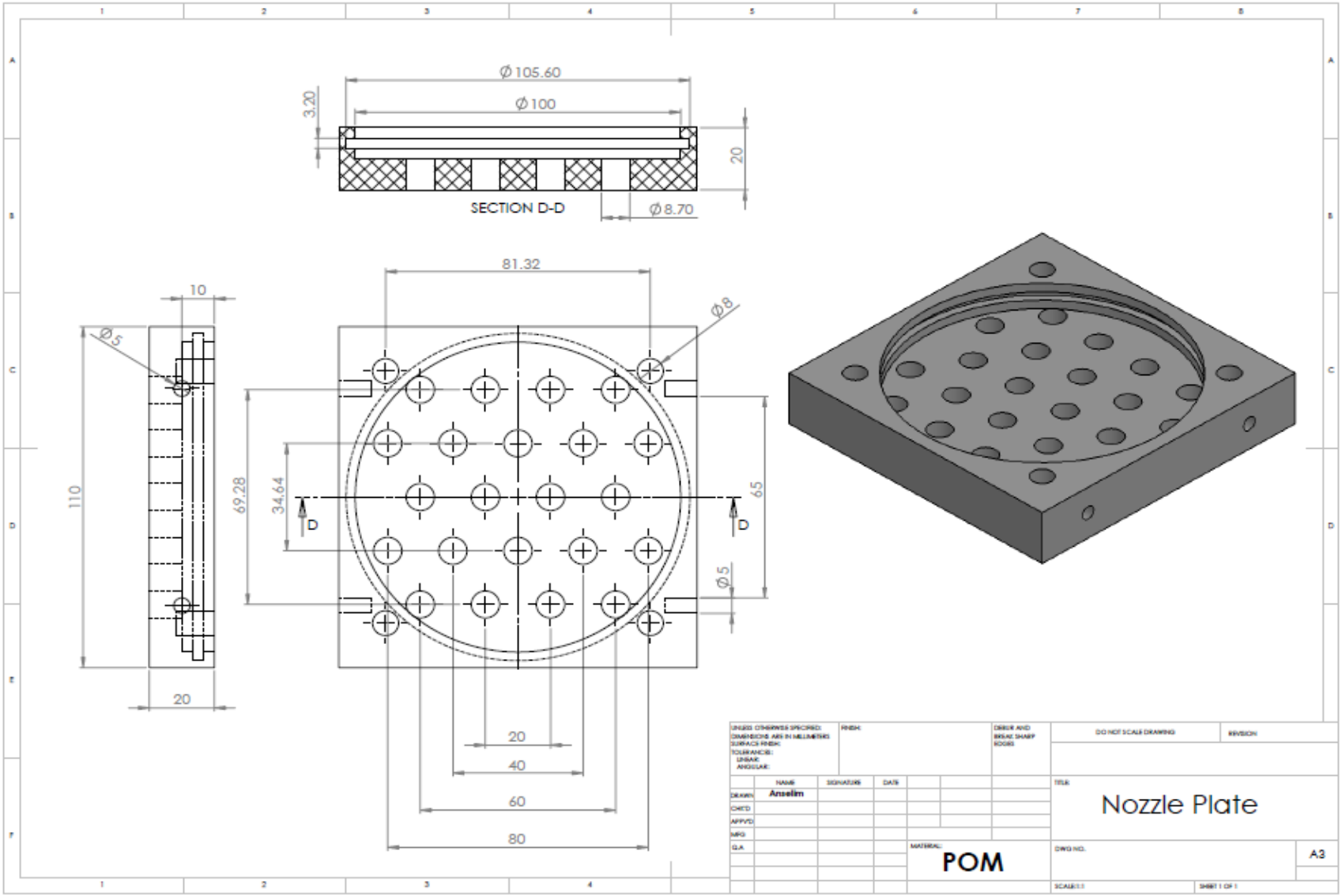

Figure 7.4: Nozzle Plate

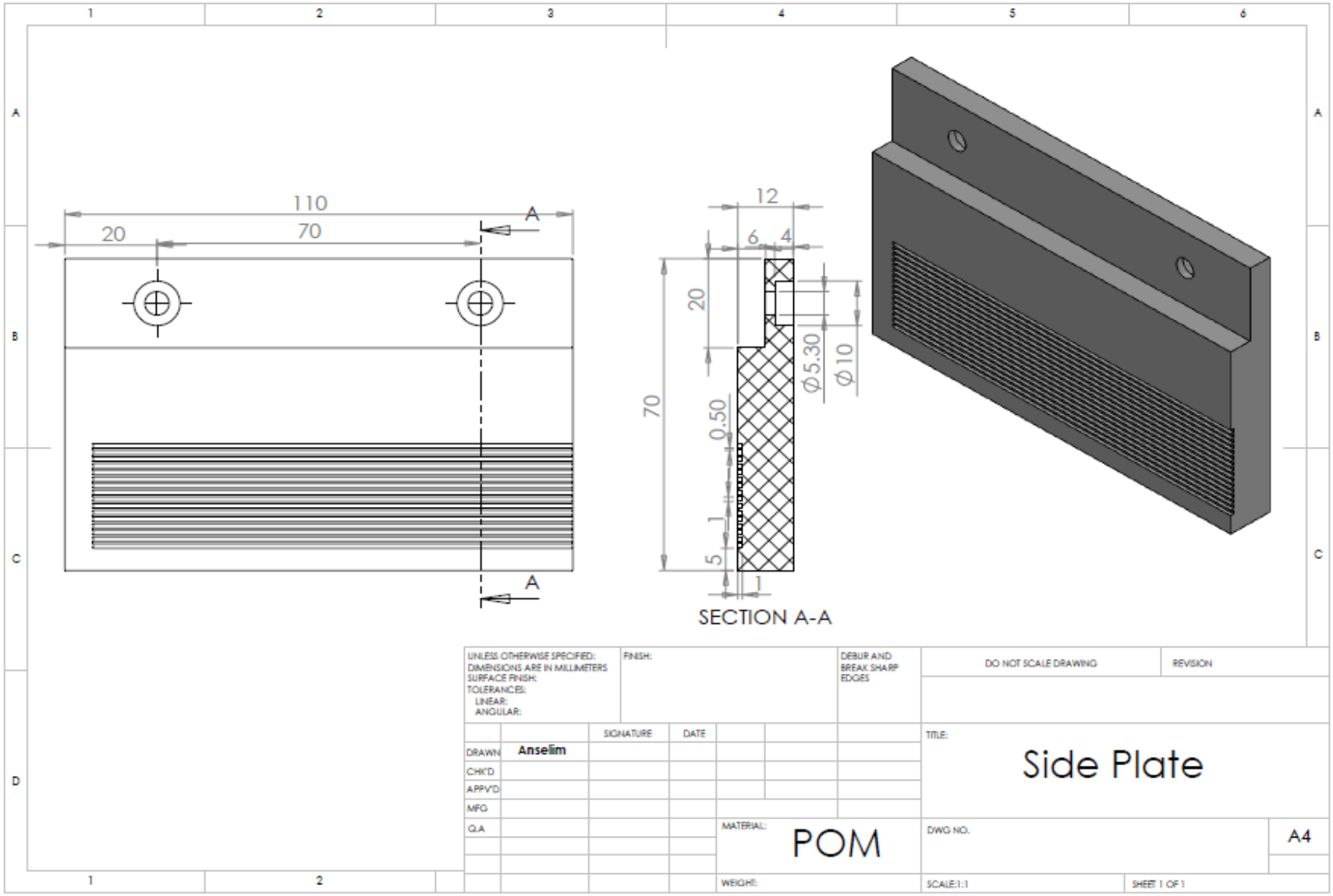

Figure 7.5: Side Plate

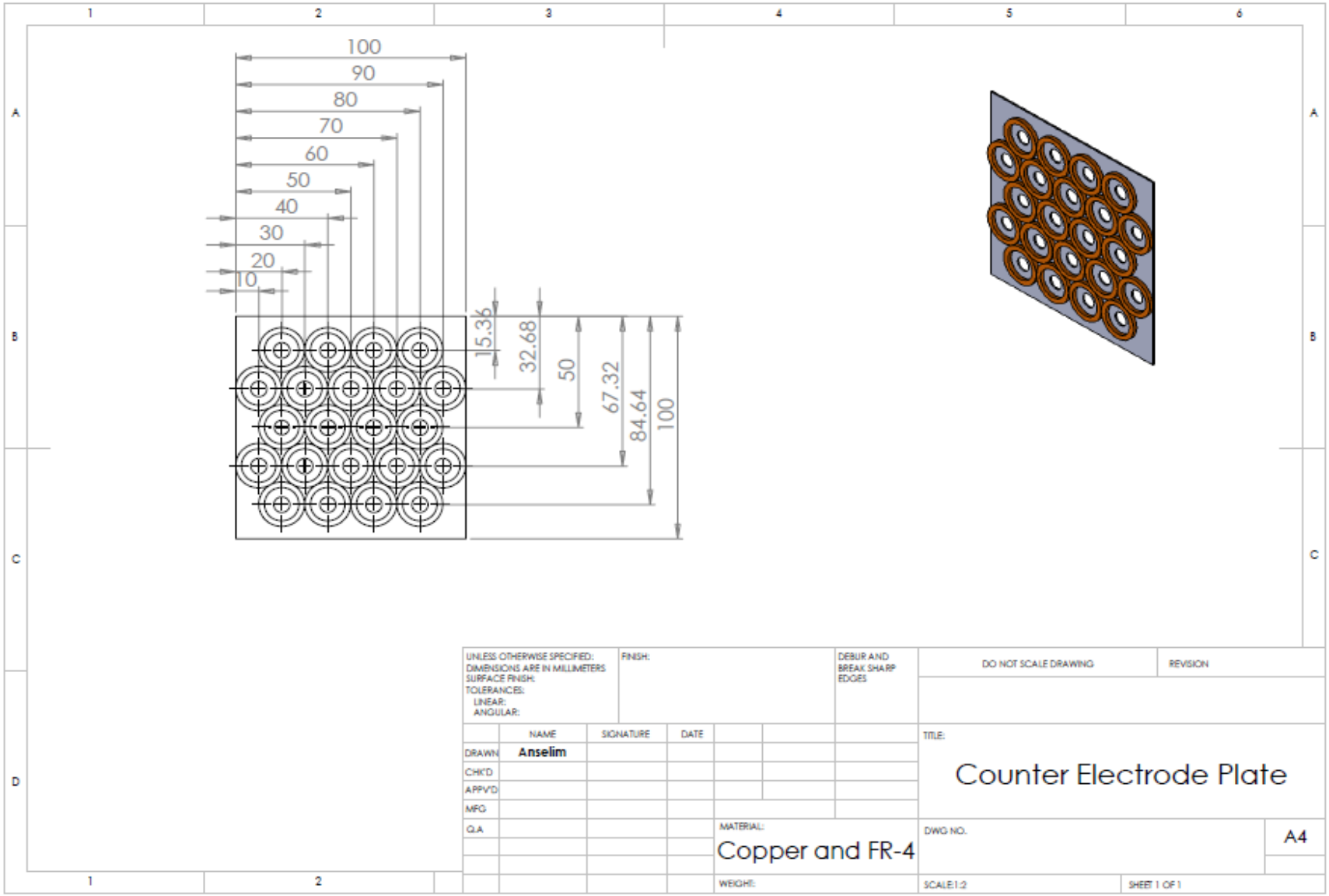

Figure 7.6: Counter Electrode Plate